

1 **Future water storage changes over the Mediterranean, Middle East, and North Africa in**  
2 **response to global warming and stratospheric aerosol intervention**

3 **Abolfazl Rezaei<sup>1,2</sup>, Khalil Karami<sup>3</sup>, Simone Tilmes<sup>4</sup>, John C. Moore<sup>5</sup>**

4 <sup>1</sup> Department of Earth Sciences, Institute for Advanced Studies in Basic Sciences (IASBS), Zanjan  
5 45137-66731, Iran. [arezaei@iasbs.ac.ir](mailto:arezaei@iasbs.ac.ir); [abolfazlrezaei64@gmail.com](mailto:abolfazlrezaei64@gmail.com).

6 <sup>2</sup> Center for Research in Climate Change and Global Warming (CRCC), Institute for Advanced Studies  
7 in Basic Sciences (IASBS), Zanjan 45137-66731, Iran

8 <sup>3</sup> Institut für Meteorologie, Stephanstraße 3, 04103 Leipzig, Germany. [khalil.karami@uni-leipzig.de](mailto:khalil.karami@uni-leipzig.de)

9 <sup>4</sup> National Center for Atmospheric Research, Boulder, CO, USA. [tilmes@ucar.edu](mailto:tilmes@ucar.edu)

10 <sup>5</sup> Arctic Centre, University of Lapland, Rovaniemi, 96101, Finland. [john.moore.bnu@gmail.com](mailto:john.moore.bnu@gmail.com)

11  
12 Corresponding Author: Abolfazl Rezaei, [arezaei@iasbs.ac.ir](mailto:arezaei@iasbs.ac.ir); [abolfazlrezaei64@gmail.com](mailto:abolfazlrezaei64@gmail.com).

13  
14 **Abstract**

15 Water storage plays a profound role in the lives of people across the Middle East and North Africa  
16 (MENA) as it is the most water stressed region worldwide. The lands around the Caspian and  
17 Mediterranean Seas are simulated to be very sensitive to future climate warming. Available water  
18 capacity depends on hydroclimate variables such as temperature and precipitation that will depend  
19 on socioeconomic pathways and changes in climate. This work explores changes in both the mean  
20 and extreme terrestrial water storage (TWS) under an unmitigated greenhouse gas (GHG) scenario  
21 (SSP5-8.5) and stratospheric aerosol intervention (SAI) designed to offset GHG-induced warming  
22 above 1.5 °C and compares both with historical period simulations. Both mean and extreme TWS are  
23 projected to significantly decrease under SSP5-8.5 over the domain, except for the Arabian Peninsula,  
24 particularly in the wetter lands around the Caspian and Mediterranean Seas. Relative to global  
25 warming, SAI partially ameliorates the decreased mean TWS in the wet regions while it has no  
26 significant effect on the increased TWS in drier lands. In the entire domain studied, the mean TWS is  
27 larger under SAI than pure GHG forcing, mainly due to the significant cooling, and in turn, a  
28 substantial decrease of evapotranspiration under SAI relative to SSP5-8.5. Changes in extreme water  
29 storage excursions under global warming are reduced by SAI. Extreme TWS under both future  
30 climate scenarios are larger than throughout the historical period across Iran, Iraq, and the Arabian  
31 Peninsula, but the response of the more continental eastern North Africa hyper-arid climate is  
32 different from the neighboring dry lands. In the latter case, we note a reduction in the mean TWS

33 trend under both GHG and SAI scenarios, with extreme TWS values also showing a decline compared  
34 to historical conditions.

35 **Keywords:** Mean and extreme water storage; SSP5-8.5; Stratospheric Aerosol Intervention; Global  
36 warming; MENA region, Caspian and Mediterranean Seas

37

### 38 **500-character short summary**

39 Water storage (WS) plays a profound role in the lives of people in the Middle East and North Africa  
40 and Mediterranean climate “hot spots”. Simulated is WS changed by greenhouse gas (GHG) warming  
41 with and without stratospheric aerosol intervention (SAI). WS significantly increases in the Arabian  
42 Peninsula and decreases around Mediterranean under GHG. While SAI partially ameliorates the GHG  
43 impacts, projected WS increases in dry regions and decreases in wet areas relative to the present  
44 climate.

45

### 46 **1. Introduction**

47 The Middle East and North Africa (MENA), with 6% of the world’s population, are currently among  
48 the most water-stressed regions worldwide (Fragaszy et al., 2020). The dry climate, intensifying  
49 droughts, increasing population, and water over-extraction particularly across the Middle East  
50 (World Bank, 2017), make it home to 12 of the 17 most water-stressed countries on the planet  
51 (Hofste et al., 2019). Water availability is crucial for sanitation (Reiter et al., 2004), economic activity  
52 (UNESCO, 2003), ecosystems (Shiklomanov and Rodda, 2003), and hydrological systems (Mooney et  
53 al., 2005).

54

55 The MENA region has the largest expected economic losses from climate-related water scarcity,  
56 robustly estimated at 6–14 % of Gross Domestic Product (GDP) by 2050 (World Bank, 2017). MENA’s  
57 terrestrial water storage (TWS) is being intensively extracted and may act as a flashpoint for conflict  
58 (Famiglietti, 2014). TWS incorporates all water on the land surface (snow, ice, water stored in the  
59 vegetation, river, and lake water) and in the subsurface (soil moisture and groundwater). Beyond  
60 anthropogenic activities, natural climate variability such as drought frequency affects water storage  
61 and agriculture, which then impacts food security (Fragaszy et al., 2020). The Middle East is  
62 especially prone to severe and sustained droughts due to its location in the descending limb of the  
63 Hadley circulation and associated dry and semiarid climate (Barlow et al., 2016). The 1998-2012 14-  
64 year period was the worst drought in the past 900 years (Cook et al., 2016). Because the saturated  
65 vapor pressure of air is largely controlled by temperature, any change in temperature, as well as

66 precipitation, substantially affects (Konapala et al., 2020; Ajjur and Al-Ghamdi, 2021; Hobeichi et al.,  
67 2022) the water storage capacity available to supply the increasing water demand in the region (Lian,  
68 2021). The MENA region, having both low precipitation and high evaporation, is very vulnerable to  
69 climate change (Giorgi, 2006; Lelieveld et al., 2012; Tabari and Willems, 2018; Zittis et al., 2019).  
70 MENA water storage is therefore particularly sensitive to any perturbation of the water cycle  
71 imposed by global warming.

72

73 GHG warming has already adversely affected water resources in the MENA region (Wang et al., 2018)  
74 and is simulated to intensify water competition between states (Arnell, 1999) in the future. Although  
75 global warming is expected to increase precipitation and soil moisture across MENA (Cook et al.,  
76 2020), it will decrease runoff and groundwater recharge by larger amounts (Milly et al., 2005;  
77 Shaban, 2008; Suppan et al., 2008). Using the GHG emission scenario A1B simulated by nine CMIP3-  
78 class climate models, Droogers et al. (2012) projected that 22% of the future annual water shortage,  
79 199 km<sup>3</sup> in 2050 in MENA, will be due to global warming. 17 global climate models from Coupled  
80 Model Intercomparison Project Phase 6 (CMIP6) under SSP5-8.5 simulate a significant increase in  
81 precipitation (+0.05 to 0.3  $\mp$  0.1 mm day<sup>-1</sup>) over South-Eastern Saharan Desert in NA by the end of  
82 the century (Arjdal et al., 2023). They also projected that the total soil moisture would increase over  
83 Southern Saharan Desert under the SSP5-8.5 (6 to 20%) and SSP2-4.5 (4 to 14%). Based on TWS data  
84 from eight global climate models participating in CMIP6, a broad part of the dry MENA region tends  
85 to be wetter under SSP5-8.5 over 2071-2100 (Xiong et al., 2022). GHG-driven groundwater storage  
86 depletion in the Middle East during the 21<sup>st</sup> century will far exceed that during the 20<sup>th</sup> century due  
87 to the increased evapotranspiration (ET) and reduced volume of snowmelt (Wu et al., 2020).

88

89 Although MENA's adjacent densely populated region, the Mediterranean, has a better water storage  
90 state, it is projected to substantially suffer from reduced water availability under future GHG climate  
91 scenarios (Lionello et al., 2006). This is due to both projected significant decreases in rainfall  
92 (MedECC, 2020) and large increases in demand for irrigation water by the end of the 21<sup>st</sup> century  
93 (Fader et al., 2016). The precipitation and water availability in the Mediterranean region, to the  
94 northwest of the MENA, is also projected to be highly sensitive to global warming, particularly  
95 regarding water availability (Lionello et al., 2006), having the largest differences in the water  
96 availability between 1.5 and 2°C warming scenarios globally (Schleussner et al., 2016). Global  
97 warming decreases Mediterranean groundwater recharge according to simulations under the IPCC  
98 A2 and B2 scenarios simulated using ECHAM4 and HadCM3 models (Döll and Flörke, 2005). Runoff

99 is decreased by 10-30% according to 12 models such as CCSM3, and ECHAM5/MPI-OM (Milly et al.,  
100 2005), and soil moisture z-scores (obtained by taking the difference from the average and then  
101 dividing it by the standard deviation of the time series from the baseline period) by -1 to -4 in warm  
102 seasons according to simulations under SSP1-2.6, SSP2-4.5, SSP3-7.0, and SSP5-8.5 (Cook et al.,  
103 2020). Water availability in turn is lowered by 8-28% for a warming of 2 °C as simulated by 11  
104 CMIP5-class models by Schleussner et al. (2016). Likewise, Döll et al. (2018) found a strong drying in  
105 the Mediterranean region under global warming since the largest precipitation decreases worldwide  
106 were simulated in this region under SSP1-2.6, SSP2-4.5, SSP3-7.0, and SSP5-8.5 scenarios (Cook et  
107 al., 2020). CMIP5 model results also confirm that the global warming (RCP2.6 and RCP6.0)  
108 substantially decreases the TWS in the Mediterranean by the mid- (2030-2059) and late- (2070-  
109 2099) twenty-first century (Pokhrel et al., 2021).

110

111 If global mean surface temperature rises to exceed 1.5 °C above the preindustrial mean temperature,  
112 severe global consequences, and societal problems can be expected (Masson-Delmotte, 2022). Solar  
113 radiation modification (SRM), a form of intervention to cool the climate by reflecting sunlight, has  
114 been proposed as a potential method of limiting global temperature rises and the associated impacts  
115 of increased GHG emissions. SRM may be the only way to keep or reduce surface temperatures to 1.5  
116 °C given the reality of the GHG mitigation measures that have been agreed upon to date (MacMartin  
117 et al., 2022). Simulations have shown a 2% decrease in total solar irradiance roughly offsets global  
118 warming due to a doubling of CO<sub>2</sub> concentrations, and continuous injections of 10-18 Tg SO<sub>2</sub> per year  
119 would lead to a cooling of about 1 °C after several years (WMO, 2022). This is consistent with  
120 observed surface cooling after large volcanic eruptions, such as the 1991 Mt Pinatubo eruption which  
121 produced cooling of about 0.3 °C over a 2-3 year period (e.g., IPCC, 2021).

122

123 Many global climate models have simulated SRM in the form of stratospheric aerosol intervention  
124 (SAI). Model studies include the Stratospheric Aerosol Geoengineering Large Ensemble Project  
125 GLENS (e.g., Cheng et al., 2019; Simpson et al., 2019; Abiodun et al., 2021), the Geoengineering Model  
126 Intercomparison Project (Kravitz et al., 2013; Tilmes et al., 2013), as well as others (e.g., Bala et al.,  
127 2008; Jones et al., 2018; Muthyala et al., 2018). Compared with global warming, SAI decreases mean  
128 global precipitation (Govindasamy and Caldeira, 2000; Bala et al., 2008; Robock et al., 2008; Cheng  
129 et al., 2019; Simpson et al., 2019) as well as both the intensity and frequency of precipitation extremes  
130 caused by GHG-induced climate change (Tilmes et al., 2013; Muthyala et al., 2018). Dagon and Schrag  
131 (2016) is a rare article that focuses on the spatial variability of runoff and soil moisture responses to

132 SRM. Although solar geoengineering weakens the global hydrologic cycle (e.g., Bala et al., 2008;  
133 Tilmes et al., 2013; Ricke et al., 2023), its regional impacts are method- and strategy-dependent  
134 (Ricke et al., 2023) with potentially substantial changes in the regional precipitation patterns (Ricke  
135 et al., 2010; Tilmes et al., 2013; Crook et al., 2015; Dagon and Schrag, 2016, Tilmes et al., 2020). While  
136 differences in temperature fields vary relatively smoothly with radiative forcing, precipitation  
137 patterns are far more variable being dependent on atmosphere/ocean/land surface coupling on a  
138 wide range of spatial and temporal scales. Furthermore, SAI simulations rely on many model-specific  
139 details and parameterizations that tend to produce larger across-model differences than simulations  
140 using simpler forms of SRM (Vioni et al., 2021). While SAI may counteract the annual-mean water  
141 availability changes over land forced by GHG, it is not easy to offset the regional consequences,  
142 especially in the hydrological cycle, such as the Amazonian drying trend and its reduced precipitation,  
143 evaporation, and precipitation minus evaporation (Jones et al., 2018).

144

145 Although the MENA region and the adjacent Mediterranean region are known to be a “hot spot” for  
146 climatic change (Giorgi and Lionello, 2008; Bucchignani et al., 2018), little has been done on potential  
147 changes in TWS across MENA especially under SRM climates. This study fills that knowledge gap and  
148 explores the changes that may occur in TWS under i) a high GHG emissions scenario, ii) the same GHG  
149 scenario combined with SAI designed to globally neutralize the GHG radiative forcing, and iii)  
150 compares both future climates with the historical conditions (1985-2014) across the Mediterranean,  
151 Middle East, and northern Africa (NA).

152

## 153 **2. Data and Methods**

### 154 **2.1. Study Area**

155 The study area is composed of MENA and southern Europe to its north including the Caspian  
156 and Mediterranean Seas. MENA covers the large region from Morocco in the west to Iran in the east,  
157 containing all the Maghreb and the Middle Eastern countries from the 15°N to 45°N latitude and from  
158 20°W to 63°E longitude (Fig. 1). As well as a water-stressed region, MENA, is a worldwide hot spot  
159 for exacerbated extreme temperatures, aridity conditions, and drought (Giorgi and Lionello, 2008;  
160 Bucchignani et al., 2018). According to the Koppen Climate Classification System (Peel et al., 2007),  
161 MENA broadly has a hot and arid climate except for the coastal regions and highlands. Most of NA has  
162 a desert climate and 90% is covered by the Saharan Desert. The 2 m air temperature rises to 50°C in  
163 summertime while the annual mean precipitation is less than 25 mm (Faour et al., 2016). The Arid

164 Steppe climate predominates in Morocco, Algeria and Tunisia with cold winters (Faour et al., 2016)  
165 except for the Atlas Mountains which are cooler and wetter (annual mean precipitation of ~500 mm).  
166

167         Across the Middle East, the largest amount of precipitation falls in four main regions: the  
168 coastal eastern Mediterranean Sea, the south coast of the Caspian Sea, the western sides of the Zagros  
169 Mountains across Iran and Iraq, and the southern tip of the Arabian Peninsula. The Middle East also  
170 contains several major deserts having little to no precipitation: the Lut and Kavir deserts in the south-  
171 east and north-central regions in Iran, the Arabian Desert, the Syrian Desert, and the Negev in south-  
172 eastern corner of the Mediterranean Sea. Middle East precipitation often originates from moisture  
173 coming from the west over the Mediterranean Sea (Evans and Smith, 2006). The Red Sea and the  
174 Persian Gulf are also source regions for the heaviest precipitations across the area.

175

176         The Mediterranean area has mild wet winters and warm to hot, dry summers as well as a  
177 complicated morphology, owing to the many steep orogenic structures, distinct basins and gulfs,  
178 along with islands and peninsulas of various sizes (Lionello et al., 2006).

179

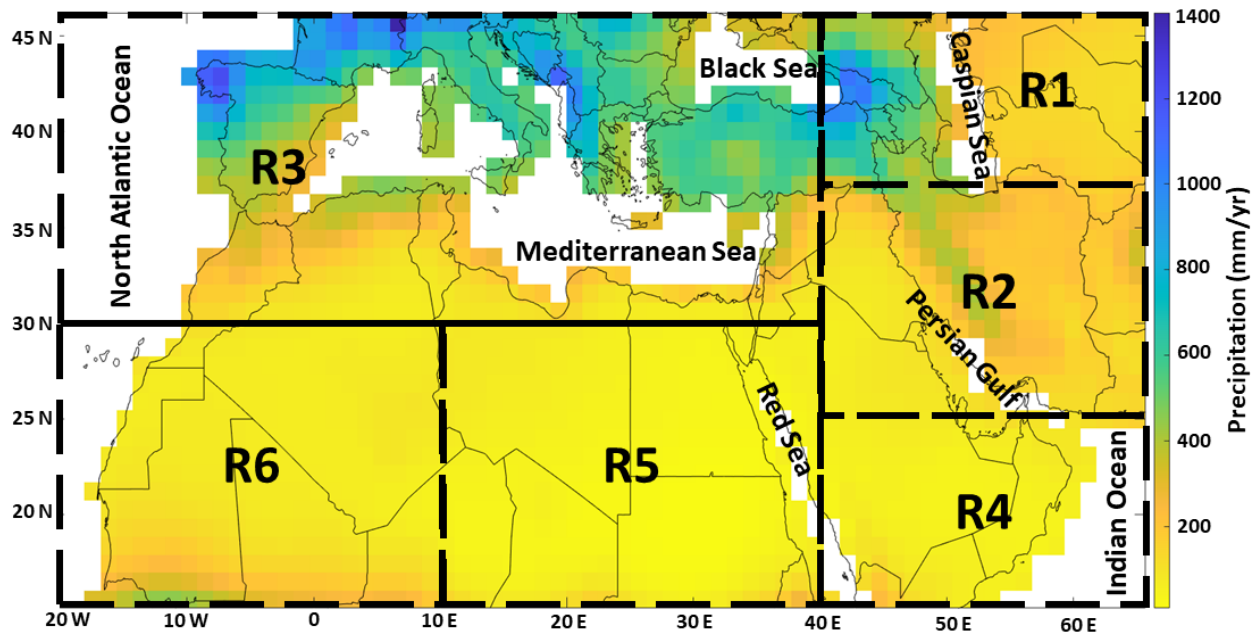
180         Based on its full range of climate types, we divided the study area into six sub-regions (R1 to  
181 R6) to explore the changes in hydroclimate variables under both global warming and SAI scenarios  
182 (Fig. 1). The regions R1 to R6 respectively refer to the lands around the Caspian Sea, eastern Middle  
183 East (largely containing Iran and Iraq), Mediterranean area, Arabian Peninsula, eastern NA, and  
184 western NA. The simulated present-day climatology (1985-2014) of each region for different  
185 hydrological quantities is summarized in Table 1. Potential evapotranspiration (ET) is the amount of  
186 evaporation that would occur if a sufficient water source were available. The Thornthwaite method  
187 was used to calculate the potential ET based on the monthly mean temperature and latitude data for  
188 each grid. Evaporation from both soil and canopy and transpiration are summed up to obtain the real  
189 ET, which is the quantity of water actually removed from a surface by evaporation and transpiration.  
190 The lands around the Caspian and Mediterranean Seas with a cooler climate, have the highest  
191 precipitation and real ET while more continental eastern NA with hyper-arid climate (with annual  
192 precipitation less than 100 mm) has the lowest precipitation, real ET, soil moisture, and TWS. The  
193 lands around the Caspian Sea have the highest soil moisture and TWS. More continental refers to an  
194 area with characteristics that are typical of continental climates and is less influenced by the  
195 moderating effects of nearby oceans.

196 **Table 1.** The medians of precipitation, temperature, real evapotranspiration (ET), soil  
 197 moisture, terrestrial water storage (TWS), and potential ET over each region (R1 to R6, see Fig. 1)  
 198 during the historical period according to the model outputs. The results for global warming and SAI  
 199 are further shown in Table S1.

Region	R1	R2	R3	R4	R5	R6
Precipitation (mm/yr)	321	182	479	78	48	112
Temperature ( $^{\circ}$ C)	14.2	20.5	17.2	27.0	23.7	25.3
Real ET (mm/yr)	419	187	388	72	50	112
Soil moisture (Kg/m <sup>2</sup> )	1846	1771	1572	1353	1155	1287
TWS (Kg/m <sup>2</sup> )	2091	1776	1623	1348	1167	1313
Potential ET (mm/yr)	74	123	74	210	143	185

200

201



202

203 **Figure 1.** The MENA's annual precipitation map during the historical period. Regions R1 to R6  
 204 largely refer to the lands around the Caspian Sea, the eastern Middle East (largely containing Iran  
 205 and Iraq), the Mediterranean area, Arabian Peninsula, eastern North Africa (NA), and western NA,  
 206 respectively.  
 207

## 208 2.2. Model simulations and scenarios

209 We examined the data from the NCAR Community Earth System Model version 2- Whole Atmosphere  
 210 Community Climate Model Version 6 (CESM2(WACCM6)) that simulated the CMIP6 (Eyring et al.,  
 211 2016) scenarios. CESM2 ranks among the top nine models known for their accuracy in simulating

212 global precipitation patterns, based on the Hellinger distance metric, which compares the bivariate  
213 empirical densities of CESM2 with those of 34 CMIP6 models, against historical precipitation data  
214 sourced from the Global Precipitation Climatology Centre (GPCC) (Abdelmoaty et al., 2021). CESM2  
215 has precipitation biases about 20% lower than CESM1 (Danabasoglu et al., 2020). CESM2(WACCM6)  
216 has an interactive stratospheric aerosol treatment (Danabasoglu et al., 2020) that is consistent with  
217 observations (Mills et al., 2016). For global terrestrial ET, the CESM2(WACCM6) ranked as the second-  
218 best model among 19 CMIP6 models (Wang et al., 2021). Furthermore, CESM2(WACCM6), reproduced  
219 the observed global land carbon trends remarkably well (Danabasoglu et al., 2020), and includes a  
220 full ocean model (Parallel Ocean Program version 2, POP2) to simulate the response of stratospheric  
221 aerosol change in the climate.

222

223 CESM2 also demonstrates satisfactory performance in simulating historical climate conditions within the  
224 study area. In the evaluation by Babaousmail et al. (2021), which assessed 15 CMIP6 models in replicating  
225 monthly rainfall patterns spanning from 1951 to 2014 in NA, CESM2(WACCM6) emerged as one of the  
226 top-performing models. It accurately captured rainfall peaks across the region, albeit with a slight  
227 overestimation (ranging from 5 to 10 mm/month) in the southern areas and a slight underestimation  
228 (ranging from 0 to 20 mm/month) in the northern regions. Despite these minor deviations,  
229 CESM2(WACCM6) was recognized as one of the models for well simulating precipitation patterns across  
230 NA, achieving a Taylor skill score of 0.62. Evaluation of CESM2(WACCM6) across the Mediterranean coasts  
231 placed it at the 9<sup>th</sup> and 17<sup>th</sup> positions out of 31 CMIP6 models for its performance in simulating  
232 temperature and precipitation (Bağçaci et al., 2021). Furthermore, when it comes to simulating  
233 precipitation relative to observational data for northeastern Iran during the period of 1987-2005, CESM2  
234 stood out as the top-performing model among six CMIP6 models (Zamani et al., 2020). Assessing the  
235 representation of spatial and temporal variations in historical precipitation from 1980 to 2014 across  
236 Africa and the Arabian Peninsula, the CMIP6 multi-mean ensemble (inclusive of CESM2(WACCM6))  
237 demonstrated reasonable performance, as highlighted in Nooni et al. (2023).

238

239 The SAI simulation we use (SSP5-8.5-SAI) is designed to employ SAI together with the high GHG  
240 emissions scenario, SSP5-8.5 with the target of limiting the mean global temperatures to 1.5°C above  
241 the pre-industrial (1850–1900) conditions (Tilmes et al., 2020). Under SSP5-8.5 forcing, Tilmes et al.  
242 (2020) projected this threshold is exceeded around the year 2020 in CESM2(WACCM6). The  
243 atmospheric component of CESM2(WACCM6) has a resolution of 1.25° in longitude and 0.9° in  
244 latitude. The experiment injects SO<sub>2</sub> at 180° longitude at four predefined latitudes (30°N, 30°S, 15°N,



245 and 15°S) at around 25 km in 15°N/S and around 22 km at 30°N/S as suggested by Tilmes et al.  
246 (2018), using a feedback control algorithm to maintain not just the global mean temperature, but the  
247 interhemispheric and equator-to-pole temperature gradients (Tilmes et al., 2020). For SSP5-8.5-SAI,  
248 most of the sulfur mass was injected at 15°S, some at 15°N and 30°S, and very little at 30°N. We used  
249 the monthly TWS (the sum of snow water equivalent and soil moisture (Wu et al., 2021)),  
250 precipitation, temperature, water evaporation from soil and canopy, transpiration, soil moisture, and  
251 leaf area index (LAI) data from all five ensemble members (r1 to r5) of the SSP5-8.5 scenario and the  
252 three available ensemble members (1-3) of SSP5-8.5-SAI. The results for variables other than TWS  
253 are shown in the Supplementary Information. For the historical period, we used all three available  
254 realizations (r1 to r3) from CESM2(WACCM6). For the anomaly analysis relative to historical  
255 conditions and the multiple linear regression models, we used the first three ensembles of SSP5-8.5,  
256 consistent with the three available historical members. We compare the GHG and SAI scenarios over  
257 2071-2100 with the 1985-2014 historical period.

258

259 We focused on the historical period from 1985 to 2014 rather than the entire historical dataset spanning  
260 from 1850 to 2100 for several reasons. Firstly, recent historical climate data may exhibit less uncertainty,  
261 given that additional meteorological stations with improved data quality are available to be used for  
262 model calibrations (Zhang et al., 2020). Secondly, this selected historical period offers valuable insights  
263 into the observable impacts of climate change, which are highly pertinent to present-day societal and  
264 environmental challenges. These insights are of utmost importance to policymakers and communities  
265 alike. Thirdly, the chosen historical 30-year time period aligns with the 30-year periods considered for the  
266 GHG emissions and SAI scenarios, ensuring consistency in our statistical analysis. We focus on the 2071-  
267 2100 future period because the anticipated changes in TWS driven by GHG emissions are expected to be  
268 more pronounced during this time frame (Pokhrel et al., 2021). Furthermore, the SAI forcing is strongest  
269 in the later period of the simulation and is expected to produce a more significant result.

270

### 271 **2.3. Return periods**

272 We are interested in climate extremes, not only changes in means. Therefore, we examine how the  
273 frequency of events of some particular levels are likely to change under different scenarios. We use  
274 the generalized extreme value (GEV) distribution function to estimate the probability distribution  
275 function of the TWS extremes. A return period is an estimated average time between events such as  
276 floods or river discharge flows. It is calculated by generating the 95% normal-approximate  
277 confidence intervals in accordance with the mean and variance of the variable (here TWS).

278 The GEV probability density and cumulative distribution functions are defined as (Gilleland, 2020):

$$279 \quad g(z) = \frac{1}{\sigma} t(z)^{1+\xi} e^{-t(z)}; \quad G(z) = e^{-t(z)}; \quad t(z) = \begin{cases} \left\{ 1 + \xi \left( \frac{z-\mu}{\sigma} \right) \right\}^{-1/\xi}, & \xi \neq 0 \\ e^{-\left( \frac{z-\mu}{\sigma} \right)}, & \xi = 0 \end{cases} \quad (1)$$

280 For  $\xi \neq 0$ , we have  $t(z)^{1+\xi} = \left\{ 1 + \xi \left( \frac{z-\mu}{\sigma} \right) \right\}^{-(1+1/\xi)}$  and for  $\xi = 0$ , the  $z$  domain restricted to

281  $\xi \left( \frac{z-\mu}{\sigma} \right) > -1$ . The GEV distribution is parameterized using  $\xi$ ,  $\mu$ , and  $\sigma$  which are the shape,

282 location, and scale parameters, respectively and analogous to the skewness, mean and standard

283 deviation. We assume that the GEV is the valid distribution function for variables  $z_1, \dots, z_n$

284 representing the annual maximum return TWS levels, where the quantiles of the distribution

285 function give the return levels,  $z_p$ . The return levels are the solutions to  $G(z_p) = 1 - p$ , which yields

286 (Gilleland, 2020):

$$287 \quad z_p = \begin{cases} \mu - \frac{\sigma}{\xi} [1 - \{-\ln(1-p)\}^{-\xi}] & \text{for } \xi \neq 0 \\ \mu - \sigma \ln\{-\ln(1-p)\} & \text{for } \xi = 0 \end{cases} \quad (2)$$

288 where  $p$  is probability corresponding to  $z_p$ . The return period is obtained as:

$$289 \quad \text{return period}(i) = 1 / (1 - \text{cdf}(i)) \quad (3)$$

290 where  $\text{cdf}$  is the cumulative distribution function. We also calculated the 95% asymptotic lower and  
291 upper confidence intervals based on the Kolmogorov-Smirnov statistic (Doksum and Sievers, 1976).

292 We used the concatenated TWS anomaly data for the historical period, high GHG emissions, and SAI

293 scenarios to analyze the return periods. As an example, the relationship between empirical quantiles

294 and model quantiles as well as the probability density versus quantiles for the regions R2 and R5 are

295 shown in Figs. S1 and S2.

296

#### 297 **2.4. Multiple linear regression (MLR) model**

298 We want to analyze how the primary driving climate fields (surface air temperature, precipitation,

299 ET, and LAI (i.e., vegetation coverage)) for TWS vary spatially and among the different scenarios

300 (Zhang et al., 2022). We use a simple multiple linear regression (MLR) model with TWS as the

301 dependent variable (Y) for each ensemble member in each region. The following procedures were  
302 conducted:

303 i) Employing the variable clustering (VARCLUS) procedure to thoroughly assess collinearity among  
304 the variables. VARCLUS is a method that effectively segregates a set of numeric variables into disjoint  
305 or hierarchical clusters, each characterized by a linear combination of the variables within the cluster  
306 (Sarle, 1990). The criterion is that when the proportion of the variance explained by a cluster is larger  
307 than 0.8, it is advisable to select one variable from that cluster. Based on the results obtained from  
308 VARCLUS (Figs. S3 and S4), we made specific decisions to enhance the robustness of our analysis. For  
309 instance, we identified strong correlations exceeding 0.9 between potential ET and temperature  
310 (Tables S2-S13 in the Supplementary Information), as well as between soil moisture and TWS in all  
311 cases (except for the eastern NA (R5) in Tables S2-S13). Consequently, we chose to exclude potential  
312 ET and soil moisture from our analysis due to their high levels of correlation with temperature and  
313 TWS, respectively.

314 ii) Considering a linear regression model with potential independent variables (X): temperature,  
315 precipitation, real ET, and LAI. We conducted a temporal autocorrelation analysis on all these  
316 independent variables for each model. This analysis was carried out using the autocorrelation  
317 function at a 95% confidence level. In all regions (except R4), the autocorrelation results indicated  
318 that the lags at the first and second months were statistically significant, while the third month lag  
319 was almost non-significant. Therefore, we modified the MLR model to include information from the  
320 two preceding months in these regions. However, in region R4, we observed different patterns. In this  
321 region, both real ET and temperature significantly depended on their respective conditions from the two  
322 previous months, while precipitation did not show this effect. Moreover, LAI in R4 exhibited  
323 dependencies on the first three and four preceding months under the SSP5-8.5 and SSP5-8.5-SAI  
324 scenarios, respectively. Consequently, we incorporated specific lagged months for each variable in  
325 R4.

326 iii) Identifying the outliers using the Bonferroni  $p$ -values (i.e., Bonferroni correlation) and then  
327 removing them. Bonferroni correlation is a modification for  $p$ -values when several dependent or  
328 independent statistical tests are being accomplished concurrently on a single data set. A Bonferroni  
329 correction divides the critical  $p$ -value by the number of comparisons being made (Bland and Altman,  
330 1995). The number of outlier data points excluded varies from zero to 5 (over the 700 point) in the  
331 36 models.

332 iv) Fitting the final model after removing the outliers. In all regions and scenarios, the MLR models  
333 are statistically significant at the 95% level. The variance explained ( $R^2$ ) varies from around 0.3 in

334 the dry southern MENA to 0.89 and 0.96 in the wetter lands around the Caspian and Mediterranean  
 335 Seas.

336 v) Assessing the relative “importance” of the variables for TWS in the final model using the Lindeman,  
 337 Merenda, and Gold (LMG) method (Lindeman et al., 1980), where the fractional variance accounted  
 338 for is determined as the independent variable-order average over average contributions in models  
 339 of different sizes. The LMG method considers the average contributions of each variable across  
 340 different model sizes and then averages these averages to provide a more robust measure of variable  
 341 importance. The LMG can be defined as (Grömping, 2007):

$$342 \quad LMG(x_k) = \frac{1}{p!} \sum_{Permutation} seqR^2(\{x_k\} | r) \quad (4)$$

343 where  $seqR^2(\{x_k\} | S_k(r)) = R^2(\{x_k\} \cup S_k(r)) - R^2(S_k(r))$  and

$$344 \quad R^2(S) = \frac{Model\ SS(model\ with\ regressors\ in\ set\ S)}{Total\ SS}$$

345 Orders have the same  $S_k(r) = S$  summarize into a single summand, we therefore can re-write  
 346 Eq. (4):

$$347 \quad LMG(x_k) = \frac{1}{p!} \sum_{S \subseteq \{x_1, \dots, x_p\} \setminus \{x_k\}} n(S)!(p - n(S) - 1)! seqR^2(\{x_k\} | S) \quad (5)$$

348 LMG has been recommended by Johnson and LeBreton (2004) and Grömping (2007) since it uses  
 349 both direct effects and impacts adjusted for other regressors in the model. As the considered  
 350 variables may be correlated with each other, when a new predictor is added to a model that already  
 351 contains other predictors, its impact can be influenced by the presence of those other variables. The  
 352 LMG method takes into account these interactions and adjusts the variable's contribution to reflect  
 353 its unique impact while considering the effects of other regressors. Importance is a unitless variable  
 354 and the sum of all independent variable importance's in each model equals the model's explained  
 355 variance. Here we use all three ensemble members separately to estimate the robustness of the  
 356 importance estimates.

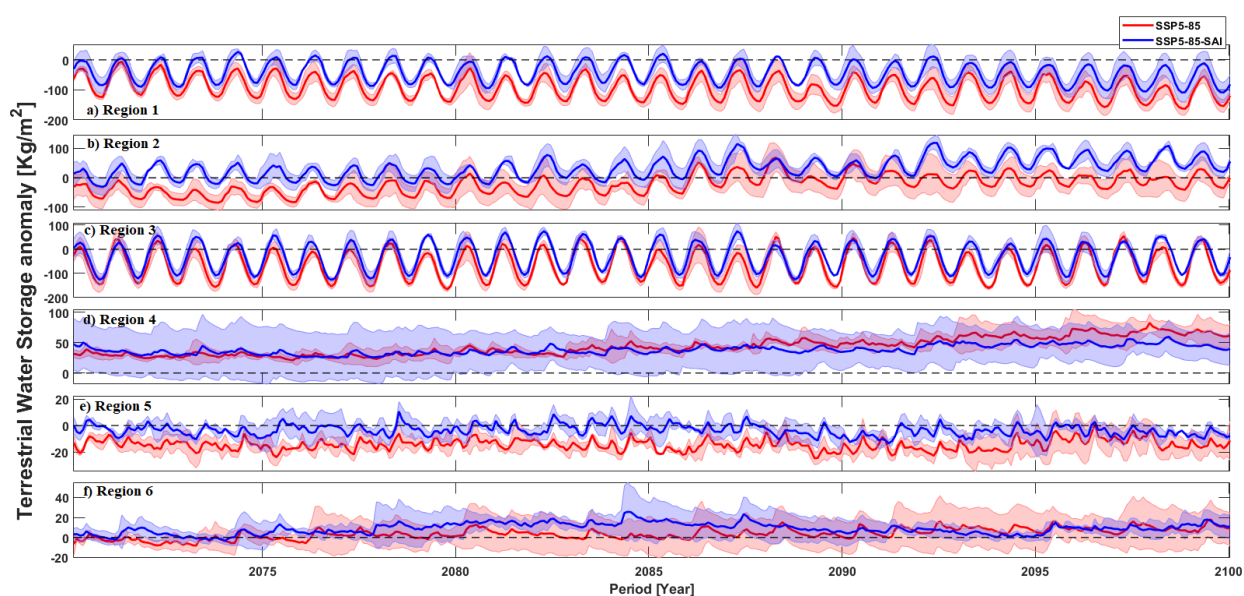
357

### 358 **3. Results:**

#### 359 **3.1. Mean terrestrial water storage (TWS) changes due to GHG and SAI**

360 In this section, we present the projected changes in TWS across MENA and the lands around the  
 361 Caspian and Mediterranean Seas. We discuss trends in the TWS anomalies relative to TWS averaged  
 362 over the historical period (1985-2014) in response to both GHG (SSP5-8.5) forcing and to GHG+SAI.  
 363 Figure 2 illustrates the original TWS anomalies, while Fig. S5 exclusively presents the long-term

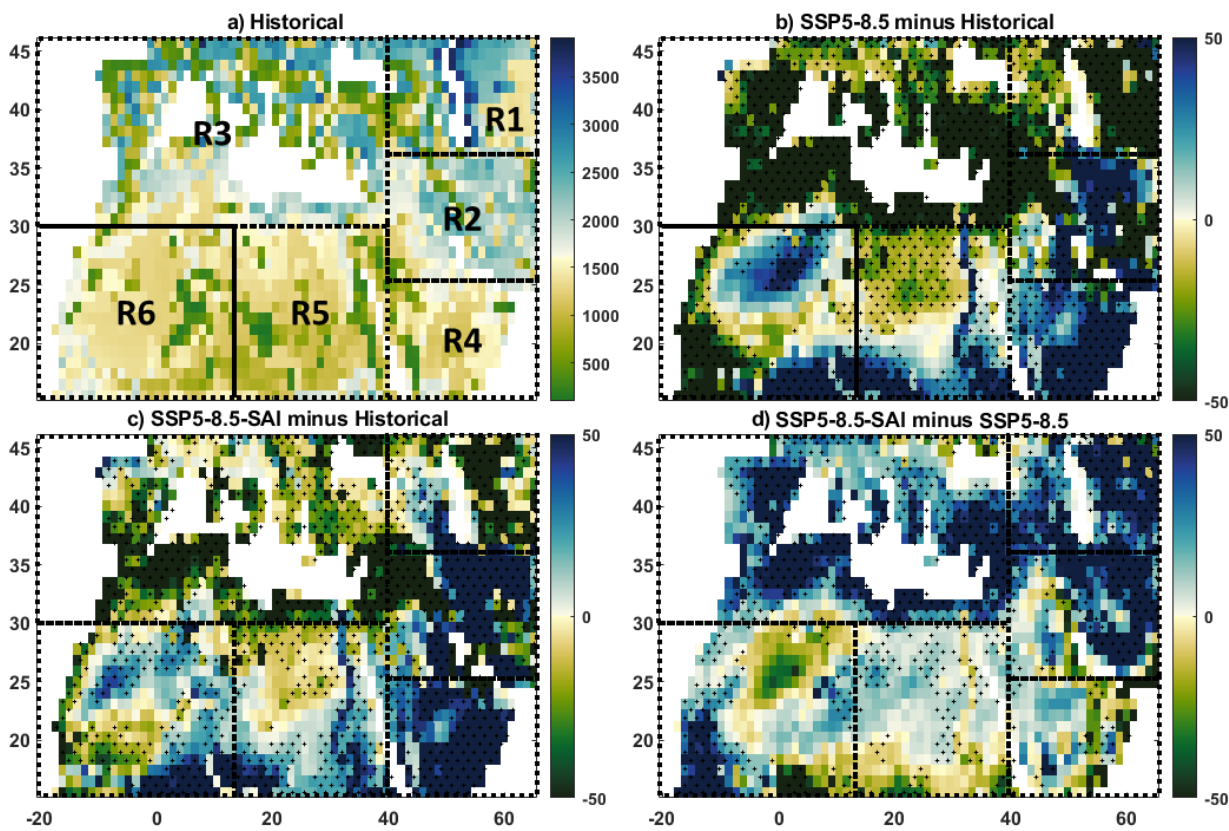
364 component, providing a clearer understanding of the changes under climate scenarios. The positive  
 365 and negative anomalies in these figures refer to increasing and decreasing TWS, respectively. The  
 366 trend decreases in the northern parts (R1 and R3) and eastern NA (R5) with a hyper-arid climate but  
 367 rises in the Arabian Peninsula (R4) and western NA (R6) under both GHG and SAI scenarios,  
 368 particularly over the latter part of the 21<sup>st</sup> century. In all regions, the SAI climate TWS is higher than  
 369 SSP5-8.5 or at least lies in the across-range of SSP5-8.5 towards the end of the century, especially in  
 370 R2 and R5 (Figs. 2 and S5). The TWS difference between SAI and global warming in the region R2,  
 371 particularly over the latter part of the 21<sup>st</sup> century, is greater relative to the rest of the domain. The  
 372 TWS change is smaller in the hyper-arid eastern NA (R5) than the other regions under both climate  
 373 scenarios.



374  
 375 **Figure 2.** The TWS anomaly relative to the TWS averaged over the historical period across MENA  
 376 and the lands around the Caspian and Mediterranean Seas under global warming without (SSP5-  
 377 8.5) and with SAI (SSP5-8.5-SAI). Figures a-f respectively are for regions R1 to R6. Shading in each  
 378 curve shows the across-ensemble range. The dashed line crossing the y-axis at zero in each subplot  
 379 is the ensemble mean of TWS over the historical period (1985-2014).

380  
 381 Figure 3 depicts the TWS differences between the historical (1985-2014) and the future climate  
 382 scenarios over the 2071-2100 period. Consistent with the above findings, Figs. 3b and S6a-c show  
 383 that the TWS response to GHG forcing in the wet regions around the Caspian (R1) and Mediterranean  
 384 (R3) Seas is simulated as declining, while across the (semi)arid MENA region, particularly in central  
 385 Iran (R2), the Arabian Peninsula (R4), and the southern portions of NA (R5 and R6), there is a positive  
 386 trend. Under global warming, the largest decrease in TWS occurs around the Caspian (particularly in  
 387 the east) and the Mediterranean (except for its north) while its most robust increase happens in the

388 southern margins of NA and the eastern parts of the Arabian Peninsula. SAI (Figs. 3c and S6d, e, and  
 389 f) partially counteracts the changes imposed by the increased GHG emission, particularly in the  
 390 wetter lands around the Caspian and Mediterranean Seas which are simulated as experiencing TWS  
 391 decrease under global warming. Temporal-ensemble mean TWS due to GHG forcing (Fig. 3b) is only  
 392 partially reversed by SAI (Fig. 3d), and the water storage shortfall is not fully canceled out by the  
 393 intervention (Fig., 3c and d). However, simulated TWS in Iran and the southern half of MENA has  
 394 greater water storage under SAI relative to the historical period (Fig. 3c).  
 395



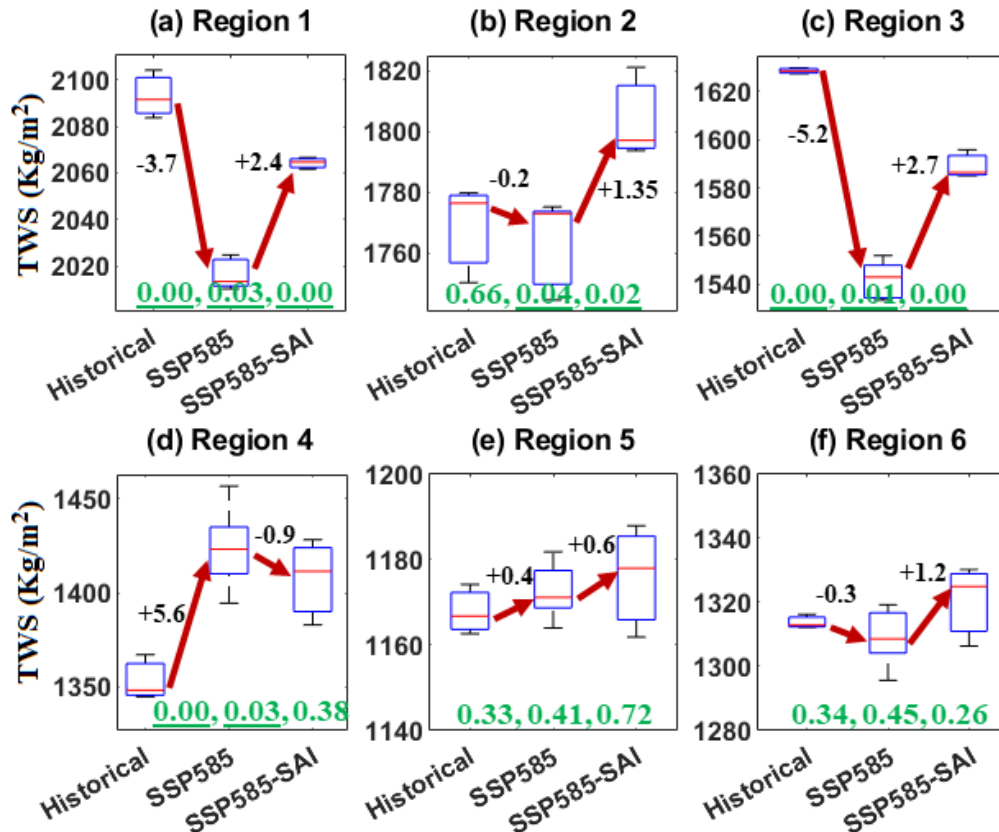
396  
 397 **Figure 3.** Ensemble mean maps of TWS across the studied domain in the historical climate (a) over  
 398 1985-2014 and their projected future changes in the 2071–2100 period under the SSP5-85 GHG  
 399 scenario (SSP5-8.5 minus historical (b) and GHG+SAI minus historical (c)). The extent to which the  
 400 SAI impacts the TWS changes imposed by global warming is further shown (SSP5-8.5-SAI minus  
 401 SSP5-8.5 (d)). Hatched areas show where all ensemble members agree on the sign of the changes.

402  
 403 In Fig. 4, we compare how simulated TWS statistical distributions vary between scenarios for each  
 404 region. Mean TWS significantly ( $p < 0.05$ ) decreases in the wetter lands around the Caspian (R1) and  
 405 Mediterranean (R3) Seas to the north (3.7-5.2% on area average) while it significantly increases in  
 406 the dry region of Arabian Peninsula (5.6%) in response to GHG warming. SAI, on the whole, partially

407 reverses the projected changes in TWS from increasing GHG concentrations toward its historical  
 408 values. Interestingly, SAI overcompensates the TWS changes imposed by the high GHG forcing in Iran  
 409 and Iraq (R2) where this region shows no significant change under GHG emissions (Fig. 4b). SAI also  
 410 has an amplifying effect in R5 and a slight overcompensation in R6, but its impact is statistically  
 411 insignificant.

412

413



414 **Figure 4.** Box and whiskers plot of the changes in the Terrestrial Water Storage (TWS) in regions 1  
 415 to 6 over 2071-2100 under SSP5-8.5 and SSP5-8.5-SAI relative to historical conditions (1985-  
 416 2014). The titles of subplots refer to the regions. The median for each experiment is denoted by the  
 417 red line, the upper (75<sup>th</sup>) and lower (25<sup>th</sup>) quartiles by the top and bottom of the box, and ensemble  
 418 limits by the whisker extents. The positive/negative values in black are the change percent under  
 419 SSP5-8.5 and SSP5-8.5-SAI relative to the median of the historical period data. The three values in  
 420 green refer to *p*-values between historical and global warming, historical and SAI, and global  
 421 warming and SAI, respectively, obtained from *t*-test analysis in which the underlined *p*-values are  
 422 statistically significant.

423

424

425 We also compared the changes in TWS with changes in precipitation, temperature, real ET, soil  
 426 moisture, and potential ET over each region under both global warming and SAI scenarios (Figs. S7  
 427 to S10 in the Supplementary Information). The TWS decreasing patterns under both SSP5-8.5 and

428 SSP5-8.5-SAI scenarios across the entire study area are similar to soil moisture change patterns (Figs.  
429 S7 and S9 in Supplementary Information), but are more widespread than precipitation under global  
430 warming (Fig. S9). Notably, in the Mediterranean and the dry MENA region, the soil moisture  
431 variability accounts for the dominant component of TWS variability (Pokhrel et al., 2021). However,  
432 the decreased TWS is seen beyond the regions of reduced precipitation (Fig. S9), from beyond the  
433 Mediterranean and Atlantic coasts to include Syria, Iraq, and the lands around the Caspian Sea as well  
434 as to a wide portion of NA (Fig. 3). These include places where precipitation is either increasing or  
435 shows no significant change, consistent with results reported by Cook et al. (2020).

436

437 In Summary, our findings show that the SSP5-8.5-SAI scenario has a potential to partially offset the  
438 significant changes in mean TWS imposed by SSP5-8.5 over the entire MENA. While SAI (Fig. 3d)  
439 succeeded in reversing mean TWS deficits in the wetter lands around the Caspian and Mediterranean  
440 Seas driven by the GHG SSP5-8.5 scenario (Fig. 3b), it did not fully cancel out the TWS deficits (Figs.  
441 3c, 4a, and 4c). However, in the dry MENA regions (Fig. 3d), particularly Iran (containing the Lut  
442 desert in the south-east region and the Kavir desert in the north-central), Iraq, and the Arabian  
443 Peninsula (housing the Arabian Desert), SAI resulted in higher mean water storage relative to the  
444 historical period (Figs. 3c and 4).

445

### 446 **3.2 Changes in extreme TWS**

447 We compared changes in the expected return frequency of comparatively rare events to those during  
448 the historical period. Changes in mean conditions discussed so far are clear, but the changes in  
449 extremes display even larger separations between those expected under pure GHG forcing and the  
450 GHG+SAI scenarios. An increase in the return level or decrease in the return period of TWS means  
451 that the rare levels of high water availability increase, while a decrease in return level for a given  
452 period means that rich water availability events become rarer. We applied a GEV distribution to the  
453 complete dataset of monthly TWS values without explicitly setting maximum values in Fig. 5. For  
454 comparison, we also extracted the annual maximum TWS values and provided the corresponding fitted  
455 GEV distribution. Overall, the probability densities for both datasets exhibit a high degree of similarity  
456 across various regions and scenarios (e.g., Figs. S11 and S12). Additionally, the graphs depicting return  
457 levels versus return periods based on annual maximums (Fig. S13) closely resemble the results obtained  
458 from the entire dataset (Fig. 5). In all cases, the trends are highly similar (compare Figs. 5 and S13),  
459 although it's worth noting that the annual maximums scenario exhibits slightly wider upper and lower  
460 bounds compared to the entire dataset scenario. We therefore focused on the results obtained from the

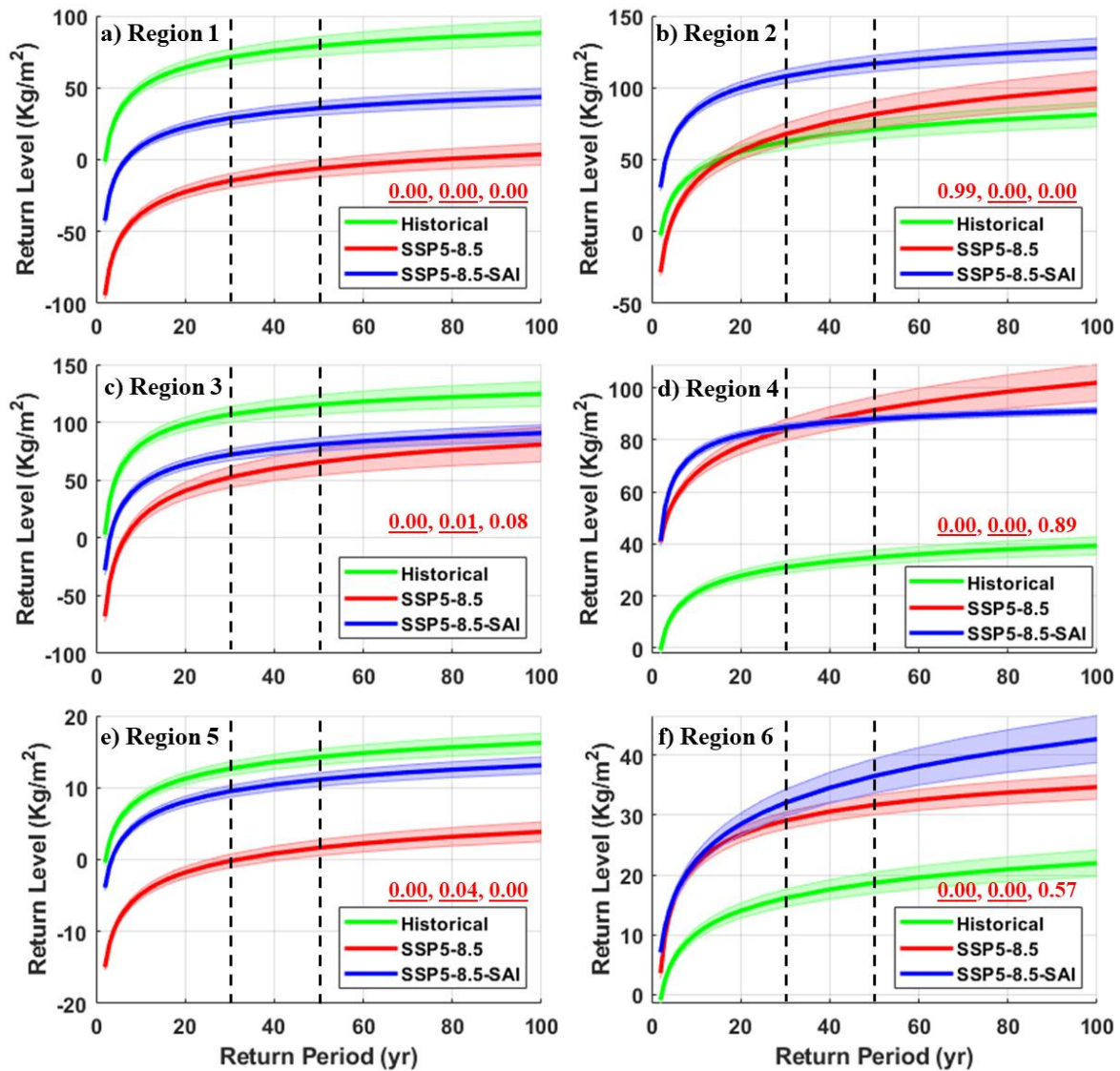


461 entire dataset. Fig. 5 shows the return levels versus return period curves with the 95% lower and  
462 upper bands. To determine which curves (including its upper and lower bounds) are significantly  
463 different from each other ( $p$ -values less than 0.05), we first conducted the repeated measures  
464 analysis of variance which compares means across one or more variables that are based on repeated  
465 observations, and then performed post hoc Tukey-Kramer comparisons. The expected return levels  
466 versus return period curves (Fig. 5) decrease in response to both GHG warming and GHG+SAI in the  
467 Caspian and Mediterranean Seas area (R1 and R3) as well as in the eastern NA (R5) as a more  
468 continental dry land but increase in the Arabian Peninsula (R4) and western NA (R6). In Iran and  
469 Iraq (R2), SAI leads to a significant increase in expected TWS return levels relative to both historical  
470 conditions and the high GHG emission scenarios (Fig. 5b) while SAI tends to partially counteract the  
471 GHG-driven TWS changes in R1, R3, R4, and R5. Larger TWS levels are expected for the entire MENA  
472 compared with the GHG climate alone, particularly in Iran, Iraq, and the western NA. Nonetheless,  
473 compared to the historical period, the Arabian Peninsula (Fig. 5d) is the region with the most robust  
474 increase in the extreme TWS under both the global warming and SAI scenarios. Extreme TWS in its  
475 neighbor dry land of eastern NA with a hyper-arid climate is still smaller than the historical  
476 conditions.

477

478 Table 2 quantitatively compares the differences between TWS (and its corresponding 95% lower and  
479 upper bounds in Fig. 5) changes at 30-, 50-, and 100-yr return periods under historical, global  
480 warming, and SAI scenarios. Global warming, on the whole, decreases the TWS extremes (i.e., fewer  
481 wetter conditions) at 30- to 100-year return periods over all the study areas except for the Arabian  
482 Peninsula (R4) and western NA (R6). The most robust decreases in the extreme TWS imposed by  
483 global warming relative to historical conditions occur in the lands around the Caspian R1 (-108% on  
484 average over return periods from 30- to 100-year) and Mediterranean R3 (-43% on average) and the  
485 eastern NA R5 (-89% on average) are partially suppressed by SAI. A small increase in the extreme  
486 TWS in Iran and Iraq (R2) simulated under GHG (+15%) is overcompensated by SAI (+65%).  
487 Although SAI decreases the TWS in the Arabian Peninsula (-11%) relative to global warming, it still  
488 tends to experience the most robust extreme water storage increases in the future (+153%)  
489 compared with historical conditions. In western NA (R6), the SAI simulation slightly intensifies the  
490 increased extreme TWS imposed by high GHG emissions by +27%. Although SAI partially  
491 compensates for the changes over most of the study area (positive SSP5-8.5-SAI minus SSP5-8.5  
492 values in Table 2), on the whole, extreme TWS tend to increase in the dry regions of Iran and Iraq,  
493 the Arabian Peninsula, and western NA while substantially decreasing in the wetter lands around the

494 Caspian and Mediterranean Seas, and to lower degrees, in the eastern NA as a more continental dry  
 495 land compared with historical conditions.  
 496



497  
 498 **Figure 5.** The TWS anomaly return level versus return period using the first three realizations for  
 499 the historical, SSP5-8.5, and SSP5-8.5-SAI in regions 1 to 6 (a to f). The two parallel dashed black  
 500 lines refer to 30- (left) and 50-year (right) return periods. Shading in each curve is the 95% upper  
 501 and lower confidence bands. The three values in red refer to  $p$ -values between historical and  
 502 global warming, historical and SAI, and global warming and SAI, respectively, obtained from the  
 503 repeated measures analysis of variance and the post hoc Tukey-Kramer comparisons in which the  
 504 underlined  $p$ -values are statistically significant.

505

506

507 **Table 2.** The percent differences (%) between the medians of the TWS return level at 30-, 50-, and 100-year return periods using the first  
 508 three realizations for the historical, SSP5-8.5, and SSP5-8.5-SAI. Consistently, the value inside the parenthesis is the percent difference-  
 509 range values between lowers and uppers 95% confidence intervals from different scenarios.

Region	(SSP5-8.5 – Historical)/Historical*100			(SSP5-8.5-SAI – Historical)/ Historical*100			(SSP5-8.5-SAI – SSP5-8.5)/ Historical*100		
	30-yr	50-yr	100-yr	30-yr	50-yr	100-yr	30-yr	50-yr	100-yr
R1	-121 (-130, -113)	-108 (-117, -100)	-96 (-105, -88)	-59 (-62, -57)	-55 (-57, -53)	-51 (-53, -49)	61 (56, 68)	53 (48, 60)	45 (40, 52)
R2	8 (6, 11)	15 (12, 17)	22 (20, 24)	73 (66, 81)	65 (58, 73)	57 (50, 65)	64 (55, 75)	50 (41, 60)	34 (25, 46)
R3	-51 (-56, -46)	-43 (-49, -38)	-35 (-42, -29)	-33 (-34, -32)	-30 (-31, -29)	-27 (-28, -26)	18 (14, 24)	13 (8, 20)	8 (2, 16)
R4	170 (163, 178)	163 (157, 169)	160 (155, 164)	173 (158, 191)	153 (138, 170)	132 (117, 150)	4 (-4, 13)	-10 (-19, 1)	-27 (-39, -14)
R5	-102 (-110, -95)	-89 (-96, -82)	-76 (-83, -70)	-25 (-26, -24)	-22 (-23, -21)	-19 (-20, -18)	77 (70, 84)	67 (61, 73)	57 (52, 63)
R6	80 (73, 89)	70 (63, 77)	58 (52, 65)	99 (95, 103)	95 (93, 99)	94 (93, 96)	18 (14, 22)	26 (21, 30)	36 (31, 41)

510

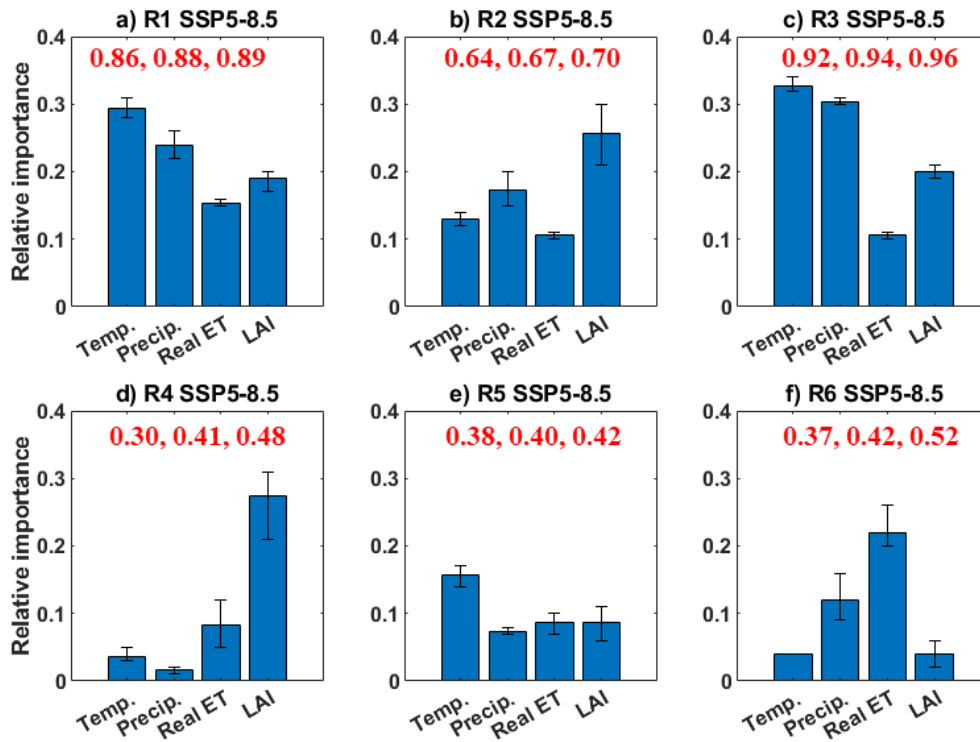
511

### 512 3.3 Drivers of TWS change

513 To assess which variables have the most impact on mean TWS under both global warming and SAI,  
514 we fitted an MLR model to each ensemble member separately in each of the six regions (Figs. 6 and  
515 7). The most important variable for the mean TWS under both global warming and SAI scenarios is  
516 region-specific. In the wet lands surrounding the Caspian (R1) and Mediterranean (R3) Seas,  
517 temperature and precipitation are the primary drivers of TWS changes. In contrast, in the Middle  
518 East, characterized by predominantly dry climates (R2 and R4), vegetation coverage (i.e., LAI) plays  
519 a dominant role. This observation aligns with the fact that temperature limits ET in the wet regions,  
520 while in arid and hot regions, the availability of water for ET is the predominant limiting factor (Bao  
521 et al., 2021). In NA, where TWS changes are irregular (Fig. 2), temperature holds the greatest  
522 significance in the eastern regions (R5), while real ET is the primary driver in the west (R6). Warmer  
523 climate enhances the atmospheric water content over regions and seasons (Cook et al., 2020) since  
524 1°C warming is accompanied by ~7% enhancement in the air water storage capacity (Trenberth,  
525 2011), and, in turn, increases the evaporative demand (Arnell, 1999), and vice versa for cooler  
526 conditions. Real ET itself is mostly controlled by temperature and available water for evaporation  
527 (i.e., precipitation, soil moisture, and vegetation coverage). With just temperature and precipitation  
528 as independent variables, we find that the temperature under both global warming and SAI is  
529 generally more important for TWS than precipitation over the wet lands around the Caspian and  
530 Mediterranean Seas as well as the eastern NA. In contrast, precipitation plays a stronger role on TWS  
531 in Iran, Iraq, and the western NA with lower precipitation under both future climate scenarios.

532  
533 The regression models indicate that TWS is mostly driven by the combined impacts of changes in  
534 vegetation coverage, real ET, temperature and precipitation, consistent with the fact that  
535 precipitation is not the only controlling factor for water resources (Cook et al., 2014; Wu et al., 2020).  
536 However, the temperature in the Mediterranean area with the highest precipitation over the entire  
537 domain studied plays a more important role than precipitation, vegetation coverage, and real ET  
538 under both warming and SAI scenarios.

539  
540 Caution is required when interpreting the relative importance results for the arid regions of R4 to R6  
541 as their variance explained ( $R^2=0.3$  to  $0.52$ ) from the MLR models is smaller than those (up to  $0.89$   
542 and  $0.96$ ) for the wetter lands around the Caspian and Mediterranean Seas. This, most probably,  
543 arises from the arid to hyper-arid climate of R4 to R6 with a small and irregular annual precipitation,  
544 and, in turn, irregular TWS anomaly time series (Figs. 2d, e, and f).



546

547

548

549

550

551

552

**Figure 6.** LMG importance plot (Lindeman et al., 1980) of the four independent variables in the regression for TWS for the global warming SSP5-8.5 scenario in each region. The bar and range-bar respectively show the ensemble mean importance and the range of importance from the three ensemble members. The three values in red on each subplot shows the minimum, mean, and maximum variances explained by models.

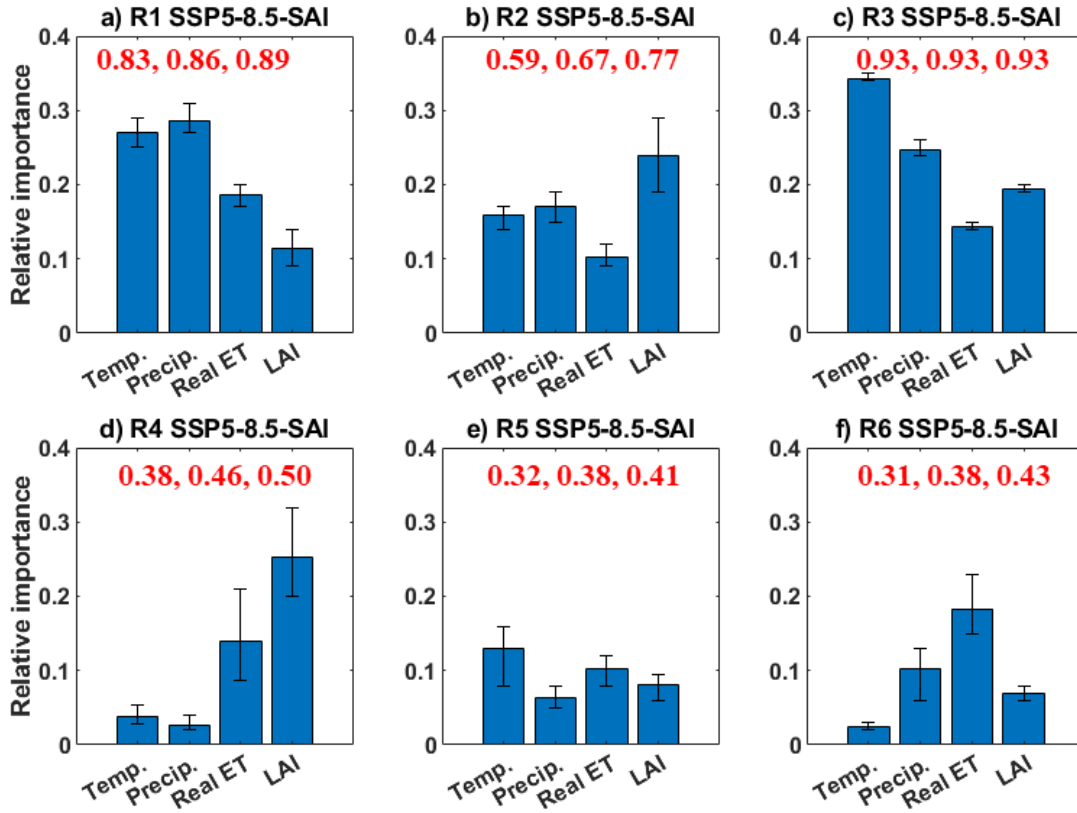


Figure 7. As in Fig. 6, but for the SSP5-8.5-SAI scenario.

553

554

555

#### 556 4. Discussion

557 We have analyzed the potential impacts of the unmitigated global warming SSP5-8.5 scenario (GHG)  
 558 and the same GHG emissions trajectory with the addition of SAI (GHG+SAI) on both the mean and  
 559 extreme water storage across the lands around the Caspian and Mediterranean Seas, Middle East,  
 560 and NA. We have used the CESM2(WACCM) climate model simulations with three realizations of each  
 561 historic and SSP5-8.5-SAI scenario and five available realizations for SSP5-8.5. In response to high  
 562 GHG emission over the 2071-2100 period, the mean TWS decreases in the wetter regions (i.e., around  
 563 the Caspian and Mediterranean Seas with mild wet winters and warm to hot, dry summers), in  
 564 agreement with the previous studies based on SSP5-8.5 (e.g., Cook et al., 2020; Scanlon et al., 2023),  
 565 RCP2.6 and RCP4.5 (e.g., Döll et al., 2018) as well as with projections from 11 global hydrological  
 566 models (Schewe et al., 2014) with globally forced 2°C warming (Schleussner et al., 2016). Similarly,  
 567 a decrease in precipitation (Kim and Byun, 2009), surface runoff (Cook et al., 2020), and TWS  
 568 (Pokhrel et al., 2021) has been reported across Mediterranean coasts under GHG warming. In  
 569 contrast, the mean TWS increases or shows no significant change in the MENA, housing several major  
 570 deserts with minimal precipitation. The temporal-ensemble mean TWS increase in the southern

571 MENA is consistent with other climate model simulations showing increased precipitation and soil  
572 moisture in CMIP6 simulations under SSP5-8.5 (Cook et al., 2020), and SSP2-4.5 (Ajjur et al., 2021;  
573 Scanlon et al., 2023). This further aligns with a projected northward shift of the inter-tropical  
574 convergence zone (ITCZ) in eastern Africa, mostly during a months of May to October (Mamalakis et  
575 al., 2020), leading to increased moisture transfer to the Southern Middle East and NA (Waha et al.,  
576 2017).

577

578 Given the prevailing water scarcity challenges in many regions of the Middle East where population  
579 growth is a continuing concern (Oroud, 2008), by mitigating the vulnerability to global warming, SAI  
580 may offer a potential strategy to augment the regional water resources across the area, particularly  
581 in the dry regions of Iran (containing the Lut desert in the south-east region and the Kavir desert in  
582 the north-central), Iraq, and the Arabian Peninsula (housing the Arabian Desert), as compared with  
583 the pure GHG forced scenario. Similarity, Jones et al. (2018) found that SAI could effectively  
584 counteract the changes in available water imposed by global warming on Earth's lands. Mousavi et  
585 al. (2023) also found increased soil moisture and enhanced vegetation coverage would lead to the  
586 reduction of dust concentration in the MEAN region under SAI.

587

588 The more robust and widespread deficit in mean TWS compared to precipitation in the area, which  
589 is in line with results reported by Cook et al. (2020), highlights the profound roles that other  
590 variables/processes have on the increased ET such as greater atmospheric moisture demand (Dai et  
591 al., 2013, 2018) and greater vegetation water use (Mankin et al., 2019) owing to warmer conditions  
592 under global warming, consistent with regression model results. According to MLR model results  
593 (Figs. 6 and 7), the projected changes in TWS were not solely attributable to precipitation; its  
594 interplay with other factors, such as vegetation coverage, temperature, and ET play a pivotal role.  
595 The vegetation coverage as the primary variable influencing changes in TWS in the MENA region  
596 substantially increases under global warming (Figs. S14 and S15). It has an important, but often  
597 complex and uncertain, role in surface water content (Lemordant et al., 2018; Trugman et al., 2018);  
598 the denser vegetation coverage, the higher evapotranspiration rates. Furthermore, although  
599 precipitation over a broad portion of MENA is lowered under SAI relative to global warming, the  
600 mean TWS, in general, increases across a broad portion of the MENA region in response to the  
601 intervention. TWS significantly increases over Iran and Iraq under SAI compared to historical and  
602 global warming (Fig. 4b) as gains in available water from decreased temperature and, in turn, ET is  
603 largely sufficient to compensate for decreased precipitation (Figs. S8 and S10), signifying that in

604 addition to precipitation, the water storage also strongly depends on local temperature (Ajjur et al.,  
605 2021). As an example, around the Caspian Sea (R1), although the changes in precipitation imposed  
606 by global warming are simulated to have been fully restored by SAI, the temperature has not; and in  
607 turn, the TWS is not fully restored by SAI. This is consistent with MLR model results (Fig. 7a) in which,  
608 beyond the precipitation, temperature also plays an important role in TWS across R1. Other studies  
609 also found that changes in precipitation does not necessarily correlate with changes in surface water,  
610 due to differences in precipitation and evaporation responses under SAI (Irvine et al., 2016).

611  
612 Our findings, on the whole, suggest that the specific SAI scenario considered here could help water  
613 storage in the dry regions (R2, R4, R5, and R6), i.e., leads to higher soil moisture and TWS compared  
614 with both the historical conditions and pure GHG-induced global warming. Likewise, Dagon and  
615 Scharg (2017) documented a rise in mean water availability and soil moisture during a period of June  
616 to August in MENA using SolarGeo simulations, consistent with the significant reduction in daily  
617 maximum temperatures and ET across the Middle East. This works through the combined positive  
618 effects of (1) a substantial decrease in temperature and ET over the entire study area compared with  
619 SSP5-8.5 global warming, and (2) the increased precipitation in the southern MENA dry regions  
620 relative to historical conditions. The Middle East may therefore benefit from the water enrichment  
621 from climate change through the implementation of solar intervention (Burnell, 2021). However, the  
622 wet and colder regions, particularly around the Mediterranean coasts, may have less water storage  
623 compared with the historical period but more water relative to the GHG scenario due to a significant  
624 decrease in ET under SAI. Simpson et al. (2019) also reported a noteworthy decline of 18.5% in  
625 available water (precipitation minus evaporation) across the Mediterranean area under high GHG  
626 emissions while it has been partially reversed (only 5%) by a decrease in evaporation under SAI.

627  
628 Although SAI partially compensates for the extreme TWS changes in most of the study area, aligning  
629 with findings by Jones et al. (2018), the overall extreme TWS trend indicates an increase in dry  
630 regions of Iran and Iraq, Arabian Peninsula, and western NA. Conversely, there is a substantial  
631 decrease in extreme TWS in the wetter lands around the Caspian and Mediterranean Seas, and to  
632 lower degrees, in the eastern NA compared to historical conditions. The implications of our findings  
633 under both future climate scenarios (SSP5-8.5 and SSP5-8.5-SAI) extend beyond hydrology and  
634 water resources management. Changes in TWS have significant implications for climate adaptation,  
635 flood and drought risk management, and infrastructure planning. Some dry areas such as Iran, Iraq,  
636 and the Arabian Peninsula are projected to receive greater extreme TWS under both global warming



637 and SAI or only SAI, and these regions have suffered historically from flooding (e.g., Abbaspour et al.,  
638 2009; Ghavidel and Jafari Hombari, 2020; Dezfuli et al., 2021). The significant increase in extreme  
639 TWS enhances their flood risks. Hence, governments in these regions should plan for adaptations to  
640 water megastructures such as the dams on the large rivers of Karkheh and Karun in western Iran and  
641 the Euphrates and Tigris in Iraq, since they have been mostly designed with historical hydrology in  
642 mind.

643

644 There are several caveats and caution needed for our results. First, our findings are based on a single  
645 model simulation (CESM2) and a single scenario climate scenario SSP5-8.5 with (three available  
646 realizations) and without (five available realizations) SAI. Future studies should consider alternative  
647 SAI scenarios to explore the sensitivity of our results to model and scenario choices. The SSP  
648 scenarios include some that clearly portray undesirable futures, especially the high emissions SSP5  
649 scenarios or the regional rivalry SSP3 that illustrate the danger of unchecked climate change  
650 (MacMartin et al., 2022). There are more caveats for the SAI experiment used here (1) it deploys in  
651 2020, therefore does not simulate any plausible future, and (2) takes into account solely the high-  
652 emissions scenario SSP5-8.5 that is suitable for capturing a high “signal” compared to internal  
653 variability. This is useful for understanding the science but inconsistent with present-day projections  
654 of mitigation attempts (Burgess et al., 2020). However, while the signal is stronger under high GHG  
655 emissions, it is plausible that the directions and patterns of response would be similar in a lower-  
656 emission experiment, with the magnitude of changes roughly depending on the degree of warming  
657 being suppressed by SAI (e.g., MacMartin et al., 2022).

658

## 659 **5. Conclusions**

660 The current study is the first attempt for understanding the influence of GHG emission and SAI  
661 scenarios on both mean and extreme water storage changes over the lands around the Caspian and  
662 Mediterranean Seas, Middle East, and northern Africa under global warming and SAI scenarios  
663 compared to the historical 1985-2014 conditions. The mean TWS is projected to decrease across the  
664 wetter lands around the Caspian and Mediterranean Seas to the north (3.7-5.2% on average) but  
665 increase over the most MENA region (up to 5.6% over the Arabian Peninsula) that has a drier climate  
666 under the high GHG forcing compared to the present-day conditions.

667

668 Although the SAI tends to reverse, to a degree, the significant changes in TWS revealed by SSP5-8.5  
669 over the entire area, it significantly overcompensates for the slightly reduced TWS under the high

670 GHG scenario in Iran and Iraq. MLR model analysis of driving factors suggests that the impacts of  
671 temperature on water storage changes, like precipitation, are also important under both high GHG  
672 forcing and SAI scenarios. Although SAI mostly decreases precipitation over most of the domain, it is  
673 accompanied by higher mean TWS across the entire study area due to the cooler climate.

674

675 Although significant changes in the extreme TWS under high GHG emissions are reduced by SAI, the  
676 changes due to both future climate changes are still large relative to the historical period across a  
677 broad portion of the domain. With SAI, TWS significantly decreases in the eastern lands around the  
678 Caspian Sea while substantially increasing across the Middle East regions of Iran, Iraq, and the  
679 Arabian Peninsula. This may increase flood risks since water megastructures have been mostly  
680 designed with historical hydrology in mind. Finally, the SAI scenario appears to increase accessible  
681 water storage in the dry regions of the Middle East and northern Africa. The wetter and colder lands  
682 around the Caspian and Mediterranean Seas may have less available water compared with the  
683 historical conditions, although SAI partially ameliorates the changes imposed by global warming.

684

#### 685 **Data availability:**

686 The data for CESM2 simulations are publicly available via its website: [https://esgf-](https://esgf-node.llnl.gov/search/cmip6/)  
687 [node.llnl.gov/search/cmip6/](https://esgf-node.llnl.gov/search/cmip6/). To access these specific data via ESGF website use the Source ID =  
688 CESM2-WACCM, Experiment ID=ssp585, and Frequency = mon. The SSP5-8.5-SAI data are freely  
689 available at <https://www.earthsystemgrid.org/dataset/ucar.cgd.cesm4.geomip.ssp5.html>  
690 (<https://doi.org/10.26024/t49k-1016>).

691

#### 692 **Acknowledgments:**

693 We appreciate the financial support from the DEGREES Initiative in collaboration with the World  
694 Academy of Sciences (TWAS) under grant no. 4500443035.

695

#### 696 **Author contributions:**

697 AR: coordinated the analysis, graphics of various figures, and manuscript preparation; KK and ST:  
698 conceptualized and prepared the data; and JCM: conceptualized and coordinated the interpretation  
699 and discussion for various sections. All authors contributed to the discussion and writing.

700

#### 701 **Competing the Interest:**

702 The contact author has declared that none of the authors has any competing interests.

703

704 **Financial support:**

705 This research has been supported by the DEGREES Initiative in collaboration with the World  
706 Academy of Sciences (grant no. 4500443035).

707

708 **References:**

709 Abbaspour, K. C., Faramarzi, M., Ghasemi, S. S., and Yang, H.: Assessing the impact of climate change  
710 on water resources in Iran, *Water Resour. Res.*, 45(10),  
711 <https://doi.org/10.1029/2008WR007615>, 2009.

712 Abdelmoaty, H. M., Papalexiou, S. M., Rajulapati, C. R., and AghaKouchak, A.: Biases beyond the mean  
713 in CMIP6 extreme precipitation: A global investigation, *Earth's Future*, 9, e2021EF002196,  
714 <https://doi.org/10.1029/2021EF002196>, 2021.

715 Abiodun, B. J., Odoulami, R. C., Sawadogo, W., Oloniyo, O. A., Abatan, A. A., New, M., Lennard, Ch.,  
716 Izidine, P., Egbeyi, T. S., and MacMartin, D. G.: Potential impacts of stratospheric aerosol  
717 injection on drought risk managements over major river basins in Africa, *Clim.*  
718 *Change*, 169(3), 1-19, <https://doi.org/10.1007/s10584-021-03268-w>, 2021.

719 Ajjur, S. B., and Al-Ghamdi, S. G.: Evapotranspiration and water availability response to climate  
720 change in the Middle East and North Africa, *Clim. Change*, 166(3-4), 28,  
721 <https://doi.org/10.1007/s10584-021-03122-z>, 2021.

722 Arjdal, K., Driouech, F., Vignon, E., Chéruey, F., Manzanos, R., Drobinski, P., Chehbouni, A., and Idelkadi,  
723 A.: Future of land surface water availability over the Mediterranean basin and North Africa:  
724 Analysis and synthesis from the CMIP6 exercise, *Atmos. Sci. Lett.*, e1180,  
725 <https://doi.org/10.1002/asl.1180>, 2023.

726 Arnell, N. W.: Climate change and global water resources, *Glob. Environ. change*, 9, S31-S49,  
727 [https://doi.org/10.1016/S0959-3780\(99\)00017-5](https://doi.org/10.1016/S0959-3780(99)00017-5), 1999.

728 MedECC: Climate and Environmental Change in the Mediterranean Basin – Current Situation and  
729 Risks for the Future, First Mediterranean Assessment Report [Cramer, W., Guiot, J., Marini, K.  
730 (eds.)] Union for the Mediterranean, Plan Bleu, UNEP/MAP, Marseille, France, 632pp, ISBN  
731 978-2-9577416-0-1, doi: 10.5281/zenodo.4768833, 2020.

732 Babaousmail, H., Hou, R., Ayugi, B., Ojara, M., Ngoma, H., Karim, R., Rajasekar, A., and Ongoma, V.:  
733 Evaluation of the performance of CMIP6 models in reproducing rainfall patterns over North  
734 Africa, *Atm.*, 12(4), 475, <https://doi.org/10.3390/atmos12040475>, 2021.

735 Bağçacı, S. Ç., Yucel, I., Duzenli, E., and Yilmaz, M. T.: Intercomparison of the expected change in the  
736 temperature and the precipitation retrieved from CMIP6 and CMIP5 climate projections: A  
737 Mediterranean hot spot case, Turkey, *Atm. Res.*, 256, 105576,  
738 <https://doi.org/10.1016/j.atmosres.2021.105576>, 2021.

739 Bala, G., Duffy, P. B., and Taylor, K. E.: Impact of geoengineering schemes on the global hydrological  
740 cycle. *PNAS*, 105(22), 7664-7669, <https://doi.org/10.1073/pnas.0711648105>, 2008.

741 Bao, Y., Duan, L., Liu, T., Tong, X., Wang, G., Lei, H., Zhang, L., and Singh, V. P.: Simulation of  
742 evapotranspiration and its components for the mobile dune using an improved dual-source  
743 model in semi-arid regions, *J. Hydrol.*, 592, 125796,  
744 <https://doi.org/10.1016/j.jhydrol.2020.125796>, 2021.

745 Barlow, M., Zaitchik, B., Paz, S., Black, E., Evans, J., and Hoell, A.: A review of drought in the Middle East  
746 and southwest Asia, *J. Clim.*, 29(23), 8547-8574, [https://doi.org/10.1175/JCLI-D-13-](https://doi.org/10.1175/JCLI-D-13-00692.1)  
747 [00692.1](https://doi.org/10.1175/JCLI-D-13-00692.1), 2016.

748 Bland, J. M., and Altman, D. G.: Multiple significance tests: the Bonferroni method, *BMJ*, 310(6973),  
749 170, <https://doi.org/10.1136/bmj.310.6973.170>, 1995.

750 Bucchignani, E., Mercogliano, P., Panitz, H. J., and Montesarchio, M.: Climate change projections for  
751 the Middle East–North Africa domain with COSMO-CLM at different spatial resolutions, *Adv.*  
752 *Clim. Change Res.*, 9(1), 66–80, <https://doi.org/10.1016/j. Accre.2018.01.004>, 2018.

753 Burgess, M. G., Ritchie, J., Shapland, J., and Pielke, R.: IPCC baseline scenarios have over-projected CO2  
754 emissions and economic growth, *Environ. Res. Lett.*, 16(1), 014016, 2020.

755 Burnell, L.: Risks to global water resources from geoengineering the climate with solar radiation  
756 management (Doctoral dissertation, University of Nottingham), 2021.

757 Byun, H. R., and Wilhite, D. A.: Objective quantification of drought severity and duration, *J.*  
758 *Clim.*, 12(9), 2747-2756, [https://doi.org/10.1175/1520-](https://doi.org/10.1175/1520-0442(1999)012%3C2747:OQODSA%3E2.0.CO;2)  
759 [0442\(1999\)012%3C2747:OQODSA%3E2.0.CO;2](https://doi.org/10.1175/1520-0442(1999)012%3C2747:OQODSA%3E2.0.CO;2), 1999.

760 Cook, B. I., Mankin, J. S., Marvel, K., Williams, A. P., Smerdon, J. E., and Anchukaitis, K. J.: Twenty-first  
761 century drought projections in the CMIP6 forcing scenarios, *Earth's Future*, 8,  
762 e2019EF001461, <https://doi.org/10.1029/2019EF001461>, 2020.

763 Cook, B. I., Anchukaitis, K. J., Touchan, R., Meko, D. M., and Cook, E. R.: Spatiotemporal drought  
764 variability in the Mediterranean over the last 900 years, *J. Geophys. Res. Atmos.*, 121(5),  
765 2060-2074, <https://doi.org/10.1002/2015JD023929>, 2016.

766 Cook, B. I., Smerdon, J. E., Seager, R., and Coats, S.: Global warming and 21<sup>st</sup> century drying. *Climate*  
767 *dynamics*, 43, 2607-2627, <https://doi.org/10.1007/s00382-014-2075-y>, 2014.

768 Crook, J. A., Jackson, L. S., Osprey, S. M., and Forster, P. M.: A comparison of temperature and  
769 precipitation responses to different Earth radiation management geoengineering  
770 schemes, *J. Geophys. Res. Atmos.*, 120(18), 9352-9373,  
771 <https://doi.org/10.1002/2015JD023269>, 2015.

772 Cheng, W., MacMartin, D. G., Dagon, K., Kravitz, B., Tilmes, S., Richter, J. H., Mills, M. J., and Simpson, I.  
773 R.: Soil moisture and other hydrological changes in a stratospheric aerosol geoengineering  
774 large ensemble, *J. Geophys. Res. Atmos.*, 124(23), 12773-12793,  
775 <https://doi.org/10.1029/2018JD030237>, 2019.

776 Dai, A.: Increasing drought under global warming in observations and models. *Nat. Clim.*  
777 *Change*, 3(1), 52-58, <https://doi.org/10.1038/nclimate1633>, 2013.

778 Dagon, K., and Schrag, D. P.: Regional climate variability under model simulations of solar  
779 geoengineering, *J. Geophys. Res. Atmos.*, 122(22), 12-106,  
780 <https://doi.org/10.1002/2017JD027110>, 2017.

781 Danabasoglu, G., Lamarque, J. F., Bacmeister, J., Bailey, D. A., DuVivier, A. K., Edwards, J., Emmons, L.  
782 K., Fasullo, J., Garcia, R., Gettelman, A., Hannay, C., Holland, M. M., Large, W. G., Lauritzen, P.  
783 H., Lawrence, D. M., Lenaerts, J. T. M., Lindsay, K., Lipscomb, W. H., Mills, M. J., Neale, R.,  
784 Oleson, K. W., Otto-Bliesner, B., Phillips, A. S., Sacks, W., Tilmes, S., van Kampenhout, L.,  
785 Vertenstein, M., Bertini, A., Dennis, J., Deser, C., Fischer, C., Fox-Kemper, B., Kay, J. E.,  
786 Kinnison, D., Kushner, P. J., Larson, V. E., Long, M. C., Mickelson, S., Moore, J. K., Nienhouse, E.,  
787 Polvani, L., Rasch, P. J., Strand, W. G., and Strand, W. G.: The community earth system model  
788 version 2 (CESM2). *J. Adv. Model. Earth. Syst.*, 12(2), e2019MS001916,  
789 <https://doi.org/10.1029/2019MS001916>, 2020.

790 Dezfuli, A., Bosilovich, M. G., and Barahona, D.: A dusty atmospheric river brings floods to the Middle  
791 East. *Geophys. Res. Lett.*, 48(23), e2021GL095441, <https://doi.org/10.1029/2021GL095441>,  
792 2021.

793 Dagon, K., and Schrag, D. P.: Exploring the effects of solar radiation management on water cycling in  
794 a coupled land-atmosphere model, *J. Clim.*, 29(7), 2635-2650, [https://doi.org/10.1175/JCLI-](https://doi.org/10.1175/JCLI-D-15-0472.1)  
795 [D-15-0472.1](https://doi.org/10.1175/JCLI-D-15-0472.1), 2016.

796 Doksum, K. A., and Sievers, G. L.: Plotting with confidence: Graphical comparisons of two  
797 populations. *Biometrika*, 63(3), 421-434, <https://doi.org/10.2307/2335720>, 1976.

798 Döll, P., Trautmann, T., Gerten, D., Schmied, H. M., Ostberg, S., Saaed, F., and Schleussner, C. F.: Risks  
799 for the global freshwater system at 1.5 C and 2 C global warming, *Environ. Res. Lett.*, 13(4),  
800 044038, <https://doi.org/10.1088/1748-9326/aab792>, 2018.

801 Döll, P., Flörke, M.: Global-Scale Estimation of Diffuse Groundwater Recharge; Institute of Physical  
802 Geography, Frankfurt University: Frankfurt am Main, Germany, Available online:  
803 [https://www.uni-frankfurt.de/45217767/FHP\\_03\\_Doell\\_Floerke\\_2005.pdf](https://www.uni-frankfurt.de/45217767/FHP_03_Doell_Floerke_2005.pdf), 2005.

804 Droogers, P., Immerzeel, W. W., Terink, W., Hoogeveen, J., Bierkens, M. F. P., Van Beek, L. P. H., and  
805 Debele, B.: Water resources trends in Middle East and North Africa towards 2050. *Hydrol.*  
806 *Earth Syst. Sci.*, 16(9), 3101-3114, [http://www.hydrol-earth-syst-](http://www.hydrol-earth-syst-sci.net/16/3101/2012/hess-16-3101-2012.html)  
807 [sci.net/16/3101/2012/hess-16-3101-2012.html](http://www.hydrol-earth-syst-sci.net/16/3101/2012/hess-16-3101-2012.html), 2012.

808 Evans, J. P., and Smith, R. B.: Water vapor transport and the production of precipitation in the eastern  
809 Fertile Crescent. *J. Hydrometeorol.*, 7(6), 1295-1307, <https://doi.org/10.1175/JHM550.1>,  
810 2006.

811 Eyring, V., Bony, S., Meehl, G. A., Senior, C. A., Stevens, B., Stouffer, R. J., and Taylor, K. E.: Overview of  
812 the Coupled Model Intercomparison Project Phase 6 (CMIP6) experimental design and  
813 organization, *Geosci. Model Dev.*, 9, 1937–1958, <https://doi.org/10.5194/gmd-9-1937-2016>,  
814 2016.

815 Fader M., Shi S., Von Bloh W., Bondeau A., Cramer W.: Mediterranean irrigation under climate  
816 change: More efficient irrigation needed to compensate for increases in irrigation water  
817 requirements, *Hydrol. Earth Syst. Sci.* 20, 953–973. [https://doi.org/10.5194/hess-20-953-](https://doi.org/10.5194/hess-20-953-2016)  
818 [2016](https://doi.org/10.5194/hess-20-953-2016), 2016.

819 Famiglietti, J. S.: The global groundwater crisis. *Nat. Clim. Change*, 4(11), 945-948,  
820 <https://doi.org/10.1038/nclimate2425>, 2014.

821 Faour, G., Mhaweij, M., and Fayad, A.: Detecting changes in vegetation trends in the Middle East and  
822 North Africa (MENA) region using SPOT vegetation. *Cybergeog: European Journal of*  
823 *Geography*, <https://doi.org/10.4000/cybergeog.27620>, 2016.

824 Frigaszy, S. R., Jedd, T., Wall, N., Knutson, C., Fraj, M. B., Bergaoui, K., Svoboda, M., Hayes, M.,  
825 and McDonnell, R.: Drought Monitoring and Warning System for the Middle East and North  
826 Africa, *Bull. Am. Meteorol. Soc.*, 101(10), 904-910, [https://doi.org/10.1175/BAMS-D-18-](https://doi.org/10.1175/BAMS-D-18-0084.1)  
827 [0084.1](https://doi.org/10.1175/BAMS-D-18-0084.1), 2020.

828 Ghavidel, Y., and Jafari Hombari, F.: Synoptic analysis of unexampled super-heavy rainfall on April 1,  
829 2019, in west of Iran. *Nat. hazards*, 104(2), 1567-1580, [https://doi.org/10.1007/s11069-](https://doi.org/10.1007/s11069-020-04232-0)  
830 [020-04232-0](https://doi.org/10.1007/s11069-020-04232-0), 2020.

831 Gilleland, E.: Bootstrap methods for statistical inference. Part II: Extreme-value analysis, *J. Atmos.*  
832 *Ocean Technol.*, 37(11), 2135-2144, <https://doi.org/10.1175/JTECH-D-20-0070.1>, 2020.

833 Giorgi, F., and Lionello, P.: Climate change projections for the Mediterranean region. *Global and*  
834 *Planet. Change*, 63(2-3), 90–104. <https://doi.org/10.1016/j.gloplacha.2007.09.005>, 2008.

835 Giorgi F.: Climate change hot-spots. *Geophys. Res. Lett.*, 33, L08707,  
836 <https://doi.org/10.1029/2006GL025734>, 2006.

837 Govindasamy B., and Caldeira K.: Geoengineering Earth's radiation balance to mitigate CO<sub>2</sub>-induced  
838 climate change, *Geophys. Res. Lett.*, 27, 2141–2144,  
839 <https://doi.org/10.1029/1999GL006086>, 2000.

840 Grömping, U.: Relative importance for linear regression in R: the package relaimpo, *J. Stat. Softw.*, 17,  
841 1-27, <https://doi.org/10.18637/jss.v017.i01>, 2007.

842 Hobeichi, S., Abramowitz, G., Ukkola, A. M., De Kauwe, M., Pitman, A., Evans, J. P., and Beck, H.:  
843 Reconciling historical changes in the hydrological cycle over land, *npj Clim. Atmos. Sci.*, 5(1),  
844 17, <https://doi.org/10.1038/s41612-022-00240-y>, 2022.

845 Hofste, R. W., Reig, P., and Schleifer, L.: 17 countries, home to one-quarter of the world's population,  
846 face extremely high water stress, 2019.

847 Intergovernmental Panel on Climate Change (IPCC): Working Group I Contribution to the Sixth  
848 Assessment Report (AR6), *Climate Change 2021: The Physical Science Basis*,  
849 2021, <https://www.ipcc.ch/assessment-report/ar6/> (last access: 5 December 2022), 2021.

850 Irvine, P. J., Kravitz, B., Lawrence, M. G., and Muri, H.: An overview of the Earth system science of solar  
851 geoengineering, *Wiley Interdiscip. Rev. Clim. Change*, 7(6), 815-833,  
852 <https://doi.org/10.1002/wcc.423>, 2016.

853 Johnson, J. W., and LeBreton, J. M.: History and use of relative importance indices in organizational  
854 research. *Organ. Res. Methods*, 7(3), 238-257,  
855 <https://doi.org/10.1177/1094428104266510>, 2004.

856 Jones, A. C., Hawcroft, M. K., Haywood, J. M., Jones, A., Guo, X., and Moore, J. C.: Regional climate impacts  
857 of stabilizing global warming at 1.5 K using solar geoengineering, *Earth's Future*, 6(2), 230-  
858 251, <https://doi.org/10.1002/2017EF000720>, 2018.

859 Karami, K., Tilmes, S., Muri, H., and Mousavi, S. V.: Storm track changes in the Middle East and North  
860 Africa under stratospheric aerosol geoengineering, *Geophys. Res. Lett.*, 47(14),  
861 e2020GL086954, <https://doi.org/10.1029/2020GL086954>, 2020.

862 Kim, D. W., and Byun, H. R.: Future pattern of Asian drought under global warming scenario, *Theor.*  
863 *Appl. Climatol.*, 98(1), 137-150, <https://doi.org/10.1016/j.ejrh.2022.101191>, 2009.

864 Konapala, G., Mishra, A. K., Wada, Y., & Mann, M. E.: Climate change will affect global water availability  
865 through compounding changes in seasonal precipitation and evaporation, *Nat.*  
866 *commun.*, 11(1), 3044, <https://doi.org/10.1038/s41467-020-16757-w>, 2020.

867 Kravitz, B., Rasch, P. J., Forster, P. M., Andrews, T., Cole, J. N., Irvine, P. J., Ji, D., Kristjánsson, J. E., Moore,  
868 J. C., Muri, H. and Niemeier, U.: An energetic perspective on hydrological cycle changes in the  
869 Geoengineering Model Intercomparison Project (GeoMIP), *J. Geophys. Res. Atmos.*, 118,  
870 13,087–13,102, doi:10.1002/2013JD020502, 2013.

871 Lelieveld, J., Hadjinicolaou, P., Kostopoulou, E., Chenoweth, J., El Maayar, M., Giannakopoulos, C.,  
872 Hannides, C., Lange, M.A., Tanarhte, M., Tyrlis, E. and Xoplaki, E.: Climate change and impacts  
873 in the Eastern Mediterranean and the Middle East, *Clim. Change*, 114, 667-687,  
874 <https://doi.org/10.1016/j.envres.2022.114537>, 2012.

875 Lemordant, L., Gentine, P., Swann, A. S., Cook, B. I., and Scheff, J.: Critical impact of vegetation  
876 physiology on the continental hydrologic cycle in response to increasing CO<sub>2</sub>, *PNAS*, 115(16),  
877 4093. [https://doi.org/10.1073/](https://doi.org/10.1073/pnas.1720712115)  
878 [pnas.1720712115](https://doi.org/10.1073/pnas.1720712115), 2018.

879 Lian, X., Piao, S., Chen, A., Huntingford, C., Fu, B., Li, L. Z., Huang, J., Sheffield, J., Berg, A. M., Keenan, T.  
880 F. and McVicar, T. R.: Multifaceted characteristics of dryland aridity changes in a warming  
881 world, *Nat. Rev. Earth Environ.*, 2(4), 232-250, [https://doi.org/10.1038/s43017-021-](https://doi.org/10.1038/s43017-021-00144-0)  
882 [00144-0](https://doi.org/10.1038/s43017-021-00144-0), 2021.

883 Lindeman, R. H., Merenda, P. F., Gold, R. Z.: Introduction to bivariate and multivariate analysis (No.  
884 04; QA278, L553.). Uniq ID: 5310754 Scott, Foresman, Glenview, IL, 1980.

885 Lionello, P., Malanotte-Rizzoli, P., Boscolo, R., Alpert, P., Artale, V., Li, L., Luterbacher, J., May, W., Trigo,  
886 R., Tsimplis, M. and Ulbrich, U.: The Mediterranean climate: an overview of the main  
887 characteristics and issues. *Environ. Earth Sci.*, 4, 1-26, [https://doi.org/10.1016/S1571-](https://doi.org/10.1016/S1571-9197(06)80003-0)  
888 [9197\(06\)80003-0](https://doi.org/10.1016/S1571-9197(06)80003-0), 2006.

889 MacMartin, D.G., Vioni, D., Kravitz, B., Richter, J.H., Felgenhauer, T., Lee, W.R., Morrow, D.R., Parson,  
890 E.A. and Sugiyama, M.: Scenarios for modeling solar radiation modification. *PNAS*, 119(33),  
891 e2202230119, <https://doi.org/10.1073/pnas.2202230119>, 2022.

892 Mamalakis, A., Randerson, J.T., Yu, J.Y., Pritchard, M.S., Magnusdottir, G., Smyth, P., Levine, P.A., Yu, S.  
893 and Foufoula-Georgiou, E.: Zonally opposing shifts of the intertropical convergence zone in  
894 response to climate change. arXiv preprint arXiv:2007.00239, 2020.

895 Masson-Delmotte, Valérie, Panmao Zhai, Hans-Otto Pörtner, Debra Roberts, Jim Skea, and Priyadarshi  
896 R. Shukla: Global Warming of 1.5° C: IPCC Special Report on Impacts of Global Warming of



897 1.5° C above Pre-industrial Levels in Context of Strengthening Response to Climate Change,  
898 Sustainable Development, and Efforts to Eradicate Poverty. Cambridge University Press,  
899 <https://www.ipcc.ch/sr15/>, 2022.

900 Milly, P. C., Dunne, K. A., and Vecchia, A. V.: Global pattern of trends in streamflow and water  
901 availability in a changing climate, *Nature*, 438(7066), 347-350,  
902 <https://doi.org/10.1038/nature04312>, 2005.

903 Mooney, H., Cropper, A. and Reid, W.: Confronting the human dilemma. *Nature*, 434, 561–562,  
904 <https://doi.org/10.1038/434561a>, 2005.

905 Mousavi, S. V., Karami, K., Tilmes, S., Muri, H., Xia, L., and Rezaei, A.: Future dust concentration over  
906 the Middle East and North Africa region under global warming and stratospheric aerosol  
907 intervention scenarios, *Atmos. Chem. Phys.*, 23, 10677–10695, [https://doi.org/10.5194/acp-](https://doi.org/10.5194/acp-23-10677-2023)  
908 [23-10677-2023](https://doi.org/10.5194/acp-23-10677-2023), 2023.

909 Muthyala, R., Bala, G., and Nalam, A.: Regional scale analysis of climate extremes in an SRM  
910 geoengineering simulation, Part 1: precipitation extremes, *Curr. Sci.*, 1024-1035,  
911 <https://www.jstor.org/stable/26495197>, 2018.

912 Nooni, I.K.; Ogou, F.K.; Chaibou, A.A.S.; Nakoty, F.M.; Gnitou, G.T.; Lu, J.: Evaluating CMIP6 Historical  
913 Mean Precipitation over Africa and the Arabian Peninsula against Satellite-Based  
914 Observation, *Atmosphere*, 14, 607. <https://doi.org/10.3390/atmos14030607>, 2023.

915 Oroud, I.M.: The Impacts of Climate Change on Water Resources in Jordan. In: Zereini, F., Hötzl, H.  
916 (eds) *Climatic Changes and Water Resources in the Middle East and North Africa*. Environ.  
917 *Sci. and Eng.*, Springer, Berlin, Heidelberg. [https://doi.org/10.1007/978-3-540-85047-2\\_10](https://doi.org/10.1007/978-3-540-85047-2_10),  
918 2008.

919 Peel, M. C., Finlayson, B. L., and McMahon, T. A.: Updated world map of the Köppen-Geiger climate  
920 classification, *Hydrol. Earth Syst. Sci.*, 11, 1633–1644, [https://doi.org/10.5194/hess-11-](https://doi.org/10.5194/hess-11-1633-2007)  
921 [1633-2007](https://doi.org/10.5194/hess-11-1633-2007), 2007.

922 Pokhrel, Y., Felfelani, F., Satoh, Y., Boulange, J., Burek, P., Gädeke, A., Gerten, D., Gosling, S.N., Grillakis,  
923 M., Gudmundsson, L. and Hanasaki, N.: Global terrestrial water storage and drought severity  
924 under climate change. *Nat. Clim. Change*, 11(3), 226-233, [https://doi.org/10.1038/s41558-](https://doi.org/10.1038/s41558-020-00972-w)  
925 [020-00972-w](https://doi.org/10.1038/s41558-020-00972-w), 2021.

926 Ricke, K., Wan, J. S., Saenger, M., and Lutsko, N. J.: Hydrological Consequences of Solar  
927 Geoengineering. *Annu. Rev. Earth Planet Sci.*, 51, 447-470,  
928 <https://doi.org/10.1146/annurev-earth-031920-083456>, 2023.

929 Ricke, K. L., Morgan, M. G., and Allen, M. R.: Regional climate response to solar-radiation  
930 management. *Nat. Geosci.*, 3(8), 537-541, <https://doi.org/10.1038/ngeo915>, 2010.

931 Reiter, L., Falk, H., Groat, C. and Coussens, C. M. (eds): *From Source Water to Drinking Water:*  
932 *Workshop Summary* (National Academies Press, Washington DC, 2004),  
933 [https://nap.nationalacademies.org/catalog/11142/from-source-water-to-drinking-water-](https://nap.nationalacademies.org/catalog/11142/from-source-water-to-drinking-water-workshop-summary)  
934 [workshop-summary](https://nap.nationalacademies.org/catalog/11142/from-source-water-to-drinking-water-workshop-summary), 2004.

935 Robock, A., Oman, L., and Stenchikov, G. L.: Regional climate responses to geoengineering with  
936 tropical and Arctic SO<sub>2</sub> injections. *J. Geophys. Res. Atmos.*, 113(D16),  
937 <https://doi.org/10.1029/2008JD010050>, 2008.

938 Sarle, W.: The VARCLUS Procedure. In *SAS/STAT User's Guide* (fourth, Vol. 2, pp. 1641–1659). SAS  
939 Institute, Inc.  
940 <http://support.sas.com/documentation/onlinedoc/stat>  
941 [http://support.sas.com/docu](http://support.sas.com/documentation/onlinedoc/stat)  
942 [mentation/onlinedoc/stat](http://support.sas.com/documentation/onlinedoc/stat), 1990.

942 Schewe, J., Heinke, J., Gerten, D., Haddeland, I., Arnell, N. W., Clark, D. B., Dankers, R., Eisner, S., Fekete,  
943 B. M., ColonGonzalez, F. J., Gosling, S. N., Kim, H., Liu, X., Masaki, Y., Portmann, F. T., Satoh, Y.,  
944 Stacke, T., Tang, Q., Wada, Y., Wisser, D., Albrecht, T., Frieler, K., Piontek, F., Warszawski,  
945 L., and Kabat, P.: Multimodel assessment of water scarcity under climate change, *P. Natl. Acad.*  
946 *Sci.*, 111, 3245–3250, doi:10.1073/pnas.1222460110, 2014.

947 Shaban, A.: Impact of Climate Change on Water Resources of Lebanon: Indications of Hydrological  
948 Droughts. In: Zereini, F., Hötzl, H. (eds) *Climatic Changes and Water Resources in the Middle*  
949 *East and North Africa. Environ. Sci. Eng.*, Springer, Berlin, Heidelberg.  
950 [https://doi.org/10.1007/978-3-540-85047-2\\_11](https://doi.org/10.1007/978-3-540-85047-2_11), 2008.

951 Shiklomanov, I. A. & Rodda, J. C. (eds): *World Water Resources at the Beginning of the 21st Century*  
952 (Cambridge Univ. Press, Cambridge, 2003), ISBN: 9780521617222,  
953 <https://www.cambridge.org/0521617227>, 2003.

954 Simpson, I. R., Simone Tilmes, J. H. Richter, Ben Kravitz, D. G. MacMartin, Michael J. Mills, J. T. Fasullo,  
955 and Angeline G. Pendergrass: The regional hydroclimate response to stratospheric sulfate  
956 geoengineering and the role of stratospheric heating, *J. Geophys. Res. Atmos.*, 124(23),  
957 12587-12616, <https://doi.org/10.1029/2019JD031093>, 2019.

958 Scanlon, B.R., Fakhreddine, S., Rateb, A., de Graaf, I., Famiglietti, J., Gleeson, T., Grafton, R.Q., Jobbagy,  
959 E., Kebede, S., Kolusu, S.R. and Konikow, L.F.: Global water resources and the role of  
960 groundwater in a resilient water future, *Nat. Rev. Earth Environ.*, 1-15,  
961 <https://doi.org/10.1038/s43017-022-00378-6>, 2023.

962 Schleussner, C.-F., Lissner, T. K., Fischer, E. M., Wohland, J., Perrette, M., Golly, A., Rogelj, J., Childers,  
963 K., Schewe, J., Frieler, K., Mengel, M., Hare, W., and Schaeffer, M.: Differential climate impacts

964 for policy-relevant limits to global warming: the case of 1.5 °C and 2 °C, *Earth Syst. Dynam.*, 7,  
965 327–351, <https://doi.org/10.5194/esd-7-327-2016>, 2016.

966 Suppan, P., Kunstmann, H., Heckl, A., Rimmer, A.: Impact of Climate Change on Water Availability in.  
967 In: Zereini, F., Hötzl, H. (eds) *Climatic Changes and Water Resources in the Middle East and*  
968 *North Africa*. Environ. Sci. Eng., Springer, Berlin, Heidelberg. [https://doi.org/10.1007/978-](https://doi.org/10.1007/978-3-540-85047-2_5)  
969 [3-540-85047-2\\_5](https://doi.org/10.1007/978-3-540-85047-2_5), 2008.

970 Tabari, H., and Willems, P.: Seasonally varying footprint of climate change on precipitation in the  
971 Middle East. *Sci. Rep.*, 8(1), 4435, <https://doi.org/10.1038/s41598-018-22795-8>, 2018.

972 Tilmes, S., MacMartin, D. G., Lenaerts, J. T. M., van Kampenhout, L., Muntjewerf, L., Xia, L., Harrison, C.  
973 S., Krumhardt, K. M., Mills, M. J., Kravitz, B., and Robock, A.: Reaching 1.5 and 2.0 °C global  
974 surface temperature targets using stratospheric aerosol geoengineering, *Earth Syst. Dynam.*,  
975 11, 579–601, <https://doi.org/10.5194/esd-11-579-2020>, 2020.

976 Tilmes, S., Richter, J.H., Mills, M.J., Kravitz, B., MacMartin, D.G., Garcia, R.R., Kinnison, D.E., Lamarque,  
977 J.F., Tribbia, J. and Vitt, F.: Effects of different stratospheric SO<sub>2</sub> injection altitudes on  
978 stratospheric chemistry and dynamics, *J. Geophys. Res. Atmos.*, 123(9), pp.4654-4673, 2018.

979 Tilmes, S., Fasullo, J., Lamarque, J.F., Marsh, D.R., Mills, M., Alterskjaer, K., Muri, H., Kristjánsson, J.E.,  
980 Boucher, O., Schulz, M. and Cole, J.N.: The hydrological impact of geoengineering in the  
981 Geoengineering Model Intercomparison Project (GeoMIP), *J. Geophys. Res. Atmos.*, 118(19),  
982 11-036, <https://doi.org/10.1002/jgrd.50868>, 2013.

983 Trenberth, K. E.: Changes in precipitation with climate change. *Clim. Res.*, 47(1-2), 123-138, doi:  
984 10.3354/cr00953, 2011.

985 Trugman, A. T., Medvigy, D., Mankin, J. S., and Anderegg, W. R. L.: Soil moisture stress as a major driver  
986 of carbon cycle uncertainty, *Geophys. Res. Lett.*, 45, 6495–6503.  
987 <https://doi.org/10.1029/2018GL078131>, 2018.

988 Trautmann, T., Koirala, S., Carvalhais, N., Güntner, A., and Jung, M.: The importance of vegetation in  
989 understanding terrestrial water storage variations, *Hydrol. Earth Syst. Sci.*, 26, 1089–1109,  
990 <https://doi.org/10.5194/hess-26-1089-2022>, 2022.

991 Visioni, D., MacMartin, D. G., Kravitz, B., Boucher, O., Jones, A., Lurton, T., Martine, M., Mills, M. J., Nabat,  
992 P., Niemeier, U., Séférian, R., and Tilmes, S.: Identifying the sources of uncertainty in climate  
993 model simulations of solar radiation modification with the G6sulfur and G6solar  
994 Geoengineering Model Intercomparison Project (GeoMIP) simulations, *Atmos. Chem. Phys.*,  
995 21, 10039–10063, <https://doi.org/10.5194/acp-21-10039-2021>, 2021.

996 Waha, K., Krummenauer, L., Adams, S., Aich, V., Baarsch, F., Coumou, D., Fader, M., Hoff, H., Jobbins, G.,  
997 Marcus, R. and Mengel, M.: Climate change impacts in the Middle East and northern Africa  
998 (MENA) region and their implications for vulnerable population groups, *Reg. Environ.*  
999 *Change*, 17(6), 1623–1638., <https://doi.org/10.1007/s10113-017-1144-2>, 2017.

1000 Wang, J., Song, C., Reager, J. T., Yao, F., Famiglietti, J. S., Sheng, Y., MacDonald, G. M., Brun, F., Schmied,  
1001 H. M., Marston, R. A. and Wada, Y.: Recent global decline in endorheic basin water  
1002 storages, *Nat. Geosci.*, 11(12), 926-932, <https://doi.org/10.1038/s41561-018-0265-7>, 2018.

1003 Wang, Z., Zhan, C., Ning, L., and Guo, H.: Evaluation of global terrestrial evapotranspiration in CMIP6  
1004 models, *Theor. Appl. Climatol.*, 143, 521-531, [https://doi.org/10.1007/s00704-020-03437-](https://doi.org/10.1007/s00704-020-03437-4)  
1005 4, 2021.

1006 World Bank: Beyond Scarcity: Water Security in the Middle East and North Africa. The World Bank,  
1007 [https://reliefweb.int/report/world/beyond-scarcity-water-security-middle-east-and-](https://reliefweb.int/report/world/beyond-scarcity-water-security-middle-east-and-north-africa-enar#:~:text=growth%20and%20stability.-,Beyond%20Scarcity%3A%20Water%20Security%20in%20the%20Middle%20East%20and%20North,can%20convert%20scarcity%20into%20security.)  
1008 [north-africa-enar#:~:text=growth%20and%20stability.-](https://reliefweb.int/report/world/beyond-scarcity-water-security-middle-east-and-north-africa-enar#:~:text=growth%20and%20stability.-,Beyond%20Scarcity%3A%20Water%20Security%20in%20the%20Middle%20East%20and%20North,can%20convert%20scarcity%20into%20security.)  
1009 [,Beyond%20Scarcity%3A%20Water%20Security%20in%20the%20Middle%20East%20an](https://reliefweb.int/report/world/beyond-scarcity-water-security-middle-east-and-north-africa-enar#:~:text=growth%20and%20stability.-,Beyond%20Scarcity%3A%20Water%20Security%20in%20the%20Middle%20East%20and%20North,can%20convert%20scarcity%20into%20security.)  
1010 [d%20North,can%20convert%20scarcity%20into%20security.](https://reliefweb.int/report/world/beyond-scarcity-water-security-middle-east-and-north-africa-enar#:~:text=growth%20and%20stability.-,Beyond%20Scarcity%3A%20Water%20Security%20in%20the%20Middle%20East%20and%20North,can%20convert%20scarcity%20into%20security.), 2017.

1011 Wu, W.Y., Lo, M.H., Wada, Y., Famiglietti, J.S., Reager, J.T., Yeh, P.J.F., Ducharne, A. and Yang, Z.L.:  
1012 Divergent effects of climate change on future groundwater availability in key mid-latitude  
1013 aquifers, *Nat. Commun.*, 11(1), 3710, <https://doi.org/10.1038/s41467-020-17581-y>, 2020.

1014 Wu, R. J., Lo, M. H., and Scanlon, B. R.: The annual cycle of terrestrial water storage anomalies in CMIP6  
1015 models evaluated against GRACE data, *J. Clim.*, 34(20), 8205-8217,  
1016 <https://doi.org/10.1175/JCLI-D-21-0021.1>, 2021.

1017 United Nations Educational Scientific and Cultural Organization, UNESCO: Water for People—Water  
1018 for Life, The United Nations World Water Development Report (Berghahn Books, Oxford,  
1019 2003), 2003.

1020 Xiong, J., Guo, S., Abhishek, Chen, J., and Yin, J.: Global evaluation of the “dry gets drier, and wet gets  
1021 wetter” paradigm from a terrestrial water storage change perspective, *Hydrol. Earth Syst. Sci.*,  
1022 26, 6457–6476, <https://doi.org/10.5194/hess-26-6457-2022>, 2022.

1023 Zamani, Y., Hashemi Monfared, S. A., Azhdari Moghaddam, M., and Hamidianpour, M.: A comparison  
1024 of CMIP6 and CMIP5 projections for precipitation to observational data: the case of  
1025 Northeastern Iran. *Theor. Appl. Climatol.*, 142, 1613-1623,  
1026 <https://doi.org/10.1007/s00704-020-03406-x>, 2020.

1027 Zittis, G., Hadjinicolaou, P., Klangidou, M., Proestos, Y., and Lelieveld, J.: A multi-model, multi-scenario,  
1028 and multi-domain analysis of regional climate projections for the Mediterranean. *Reg.*  
1029 *Environ. Change*, 19(8), 2621-2635, <https://doi.org/10.1007/s10113-019-01565-w>, 2019.

1030 Zhang, X., Li, J., Wang, Z., and Dong, Q.: Global hydroclimatic drivers of terrestrial water storage  
1031 changes in different climates. *CATENA*, 219, 106598,  
1032 <https://doi.org/10.1016/j.catena.2022.106598>, 2022.

1033 Zhang, B., Xia, Y., Long, B., Hobbins, M., Zhao, X., Hain, C., Li, Y. and Anderson, M.C.: Evaluation and  
1034 comparison of multiple evapotranspiration data models over the contiguous United States:  
1035 Implications for the next phase of NLDAS (NLDAS-Testbed) development. *Agric. For.*  
1036 *Meteorol.*, 280, 107810, <https://doi.org/10.1016/j.agrformet.2019.107810>, 2020.

1037